Chapter 3

Entirely Coupled Recurrent Neural Network Based Backstepping Control for Global Stability of Power System Networks

In an interconnected power system network, global performance is affected by various unknown power system parameters subjected to system uncertainties. These unknown parameters in the control expression deteriorate the performance of the power system network. Therefore, these terms associated with the control expression must be estimated precisely. This paper proposes an adaptive backstepping scheme using an entirely coupled recurrent neural network (ECRNN) to estimate these control terms. Three continuous differentiable functions are used to design control input, virtual signals, and adaptive control laws to achieve global performance. The objective of ECRNN is to reduce the control complexity by estimating the associated nonlinear term in the control expression. It will facilitate the complex formulation of the controller and improve system performance. The robust functional estimation ability of ECRNN will make the system immune to uncertainties that may appear due to external disturbances. In ECRNN, feedback loops are added to each neuron layer to achieve additional estimation accuracy. The proposed adaptive law enhances the online weight update speed and accuracy. Verification of the proposed scheme is carried out in MATLAB/Simulink. It is also verified in the real-time digital simulator (RTDS) platform using the IEEE standard New England 39-bus, 10-machine power system model.

This chapter of the thesis is motivated by the existing limitations in the global performance of a multimachine power system network due to uncertainty in the system

parameters. Uncertainties in the power system network primarily appeared due to penetration of renewable power sources, load uncertainty, or occurrence of an uncertain fault in the network. As power system networks are complex nonlinear interconnected systems, these perturbations in the generator states may cause economic losses, load demand uncertainty, or electric scarcity. Thus, a control scheme is required to address the global performance of such networks. This article proposes uniform ultimate bounded stability of synchronous generators in a multimachine power system network with a robust ECRNN-based backstepping control design.

3.1 Introduction

Stable and reliable performance of the power system network is the main objective of current research in the context of global economic and industrialization development. Modernization of power system network must equip with the advanced topologies, which enhance the operation regime through their strong robustness and performance [44]. It can be achieved by voltage regulation and maintaining transient accuracy through the excitation control of the synchronous generators. But the penetration of renewable power sources, severe faults, and parametric uncertainty in the load demand may produce mechanical power perturbations and instability in the system to power blackout and economic losses. Uncertainties in the power system parameters directly affect the generator states and perturb global performance for interconnected power system networks. This chapter of the thesis proposes an adaptive ECRNN-based backstepping control to suppress the effect of state uncertainties and external disturbances. Conventionally, excitation generators use an automatic voltage regulator (AVR) for terminal voltage regulation through speed variation, which leads to power system oscillations. Therefore, the power system stabilizer (PSS) is designed [44],[45]. The PSS and AVR provide additional damping to the power system excitation. PSS is the conventional tool used for electromechanical damping. It is comparably easy to install for the power system generators in an efficient, practical, and cheaper sense but is limited to local stability.

Other advanced control schemes based on linear methods are LMI-based H_∞ control [46] and linear quadratic regulator (LQR) [47]. These control methods have a fixed operating region and have moderate performance when large disturbances have occurred. Nonlinear techniques are adopted to extend the stable operation regime in the power system network. Nonlinear schemes so far proposed with their specific contributions in the area of power system stability are feedback linearization (FL)[16], [17] optimal control [7], [18] passivity-based control (PBC) [48] model predictive control (MPC) [49] , sliding mode control (SMC)[17],[43],[51] and backstepping control (BC)[17],[50] and [54], for excitation. The feedback linearization scheme is categorized into partial feedback (PF) [16], exact feedback (EF) [48] and direct feedback (DF) [49] schemes. Both EF and DF linearization schemes require the exact feedback rotor angle values for the control application, limiting the practical implementation of these techniques. The PF linearization scheme can overcome the drawbacks of EF and DF linearization schemes. Although, PF linearization scheme implementation needs exact information of system parameters which are difficult to obtain accurately due to intense nonlinear generator dynamics. A nonlinear MPC scheme for unmodeled power system dynamics for excitation control is introduced. But the MPC scheme mainly relies on the prediction horizon, and due to the complex nonlinear interconnection of power system networks, it lacks accuracy in a practical scenario. The schemes PBC proposed in [51] require damping and interconnection matrices to design the controller for a multimachine power system. These matrices involve nonlinear power system terms that are difficult to calculate without a prior estimation scheme. This will result in the form of a considerable control effort during perturbations.

This chapter of the thesis proposes an ECRNN-based adaptive backstepping scheme to simplify control computation by estimating the complex nonlinear part from the control expression. This will facilitate the power system operation in a way to determine exact values of unknown control terms during the perturbation condition. Whereas in other control schemes the unknown power system parameters like inertia constant H, damping coefficient D, transient and sub-transient reactance along with the transient

open-circuit time constant T_{do} deteriorate the overall system performance.

The adaptive laws to update the respective weights of ECRNN neurons are designed, which mitigate the sensitivity of unknown power system parameters during perturbation. This will enhance the dynamic stability of the power system network. The proposed ECRNN algorithm has excellent estimation capability compared to a conventional recurrent neural network [7], backpropagation neural network, and radial basis function network [52]. Three continuously differentiable functions are used to design the ECRNN-based backstepping control law, backstepping virtual variables, and adaptive laws, which contribute the following merits:

- The complex nonlinear power system term associated with the control input is estimated through ECRNN to reduce the dynamical complexity in the control law comprehensibly.
- Adaptive laws in the ECRNN scheme are designed to tune the neurons adequately to ensure global performance with the defined continuous differentiable functions. These adaptive laws facilitate compensating the impact of deviation in the unknown power system parameters.
- This ECRNN-based robust backstepping control design adaptively suppresses the external disturbances along with the state uncertainties caused due to mechanical input power change.
- The suppression of low-frequency interarea oscillations is governed by predefined tracking accuracy a priori before the control implementation.

Remark: In the proposed ECRNN-based adaptive backstepping control design, the global performance of the interconnected power system network is ensured by the three continuously differentiable functions. With these defined continuous functions, the associate term with the control input is estimated using ECRNN algorithm. In this way, the computational burden from the control action is reduced with the global performance. Whereas the robustness of the system is ensured by the backstepping scheme. Further, the adaptive laws are designed to adequately tune the ECRNN neurons as per variations in

the unknown parameters under uncertainties.

3.2 Power System Dynamics and Control Formulation

Synchronous generators in a multimachine power system are interconnected to satisfy the required load demand. The modeling of a power system network can be done in several ways, depending on the projected applications. The excitation control of synchronous generators in a multimachine power system can be broadly modeled and expressed in a 3rd order dynamic. The synchronous generator dynamics are primarily configured by the interconnection of mechanical and electrical dynamics of i^{th} synchronous generator in a power system network having n number of generators. Synchronous generator dynamics in an electromechanical sense is described by algebraic/differential equation of the following forms with the parameters of their usual meanings:

Referring the eqns. (*2.1*)-(*2.2*) from chapter 2 represents the mechanical configuration of the synchronous generator, while eqn. (*2.3*) represents the electrical dynamics of i^{th} synchronous generator. By using eqns. (*2.4*)-(*2.9*) from chapter 2 the power system 3rd order dynamics of i^{th} synchronous generator can be represented in the as provided in eqns. (*2.1*)- (*2.3*).

Now the eqns. (*2.1*)- (*2.3*) from chapter 2 is used to design backstepping excitation control E_{fdi}. The proposed control procedure can stabilize the complete power system network under fault cases and maintain stability as desired. If the variables $x_1, x_2, and\ x_3$ are system states and $\theta_1 = -\frac{D_i}{2H_i}$, $\theta_2 = \frac{\omega_{0i}}{2H_i}P_{mi}$, $\theta_3 = -\frac{\omega_{0i}}{2H_i}$, $\theta_4 = \frac{1}{T'_{doi}}$, and $\theta_5 = \frac{(x_{di}-x'_{di})}{T_{doi}}$ then eqns. (*2.1*)- (*2.3*) from chapter 1 can be modified and written as:

$$\dot{x}_1 = x_2 \tag{3.1}$$

$$\dot{x}_2 = \theta_1 x_2 + \theta_2 + \theta_3 I_{qi} x_3 \tag{3.2}$$

$$\dot{x}_3 = -\theta_4 x_3 + \theta_5 I_{di} + \theta_4 U \tag{3.3}$$

3.3 Control Problem Formulation and Strategy

The perturbations in the mechanical power input widely affect synchronous generator state stability. Changes in the mechanical input power can occur due to the

integration of renewable power sources in the power system networks. Also, the power system's unknown parameters (such as transient time constants and reactance) play a vital role in achieving the desired stability. Any fluctuation in these parameters may cause power system instability and increase nonlinear complexity in the control topology. Therefore, it is essential to estimate the complex control associate term accordingly. The ECRNN-based backstepping control is proposed for excitation control using power system network dynamics as given in eqns. (*2.1*)- (*2.3*) in chapter 2 to attain global stability in the presence of uncertainties and disturbances. The controller is designed using three continuously differentiable switching functions of 3rd order for the error approximation in the ECRNN scheme.

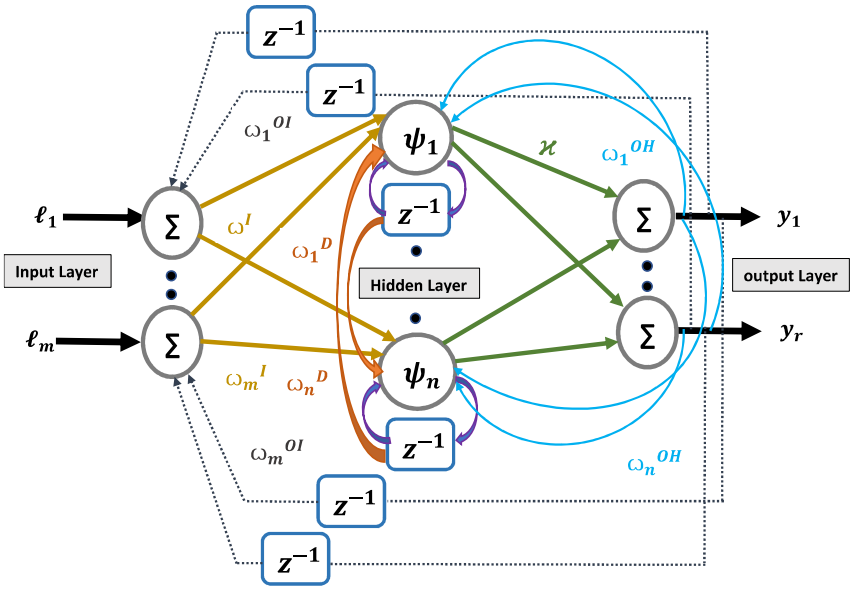

Figure 3.1. ECRNN configuration

3.3.1. Preliminaries

As per the system stability constraints, primarily lemmas, definitions, ECRNN structure, and the three continuously differentiable functions are described in this section.

3.3.1.1. Barbalat Lemma for UUB stability

Consider the system defined as:

$$\dot{x} = f(x,t), \qquad x(t_0) = x_0 \tag{3.4}$$

where the system states are $x \in R^n$ and $f: R^n \times [t_0, \infty) \to R^n$ is a continuous function. The initial state vector is $x_0 \in R^n$ at the initial time $t_0 \in [0, \infty)$.

Definition 1 [53]: if there exists $U \subset R^n$ such that for the state vector $x_0 \in U$, a positive number δ and $T(\delta, x_0)$ exists such that $\|x(t)\| < \delta$ for time $t \geq t_0 + T(\delta, x_0)$, the (*3.4*) will be UUB. Also, if $U = R^n$ then (*3.4*) should be globally UUB.

Lemma 1[53]: Let a function $V(t) \geq 0$ be defined for time for $t \in [0, \infty)$ where $V(t)$ is bounded and continuous. Now, if $\dot{V}(t) \leq -\gamma\, V\,(t) + \kappa$, then:

$$V(t) \leq V(0)e^{-\gamma t} + \frac{\kappa}{\gamma}(1 - e^{-\gamma t}). \tag{3.5}$$

Where $\kappa > 0$ and $\gamma > 0$. As $t \to \infty$, $V(t) \leq \frac{\kappa}{\gamma}$.

Lemma 2 [53]: If $f(t)$ in (*3.4*) is finite as $t \to \infty$, and also if the derivative of it, $\dot{f}(t)$ is bounded, i.e., it is uniformly continuous, then as $t \to \infty$, $\dot{f}(t) \to 0$.

Remark 1: In [52] closed-loop power system stability is proved as per Lemma 1, where a positive Lyapunov candidate $V(t)$ is designed from error variables and the parameter estimation error. Thus, the synchronous generator state errors are ensured to be UUB. However, in practice, the tracking accuracy is ensured a priori before the backstepping excitation control design. Therefore, in the proposed scheme, an adaptive ECRNN-based backstepping control is designed as per Lemma 2 rather than Lemma 1.

3.3.1.2. ECRNN Configuration

The ECRNN structure is depicted in Figure 3.1. In this configuration, all neurons receive feedback from the other respective neurons. The ECRNN is configured with input, output, and hidden layers. The coupling in the hidden layer contains self-feedback and information from other hidden layer neurons. Hidden layer neurons also have feedback connections through the neurons of the output layer. Four feedback signals enhance the accuracy of ECRNN, hidden layer neurons from self-feedback, other hidden layer neurons, output neurons, and the input neurons.

Similarly, the input layer in ECRNN has feedback from the output neurons. These feedback signals in ECRNN perform as a memory element to improve the capture ability of dynamic power system characteristics in ECRNN [54]. The ECRNN layer structure with the description of concern weights is described below:

ω_m^I Input to hidden layer weights

ω_m^{OI} Output to input layer weights

ω_n^D Delayed hidden layer self-loop weights

$\varkappa$ Hidden layer to output weights

ω_n^{OH} Output to hidden layer weights

1) Input layer in ECRNN: The layer of ECRNN input contains m number of neurons and a weighted sum of feedback from the output with the corresponding input neurons. The input is expressed as:

$$\mathcal{J}_i = f_i\left(\ell_i + \sum_{a=1}^{r} e\ell_y(a)\omega_{ia}^{OI}\right) = \ell_i + \sum_{a=1}^{r} e\ell_y(a)\omega_{ia}^{OI} \tag{3.6}$$

where $i = \{1, 2, \ldots, m\}, \ell_i \in R^m$ are the inputs, r denotes the number of outputs, $e\ell_y(a) = z^{-1}(y_a) \in R^r$. Here z^{-1} is the single step delay, and $\omega^{OI} \in R^{m\times r}$ is the weighted feedback from output layer to input layer.

2) Hidden Layer in ECRNN: The n number of neurons is considered in the hidden layer of the ECRNN structure. These neurons receive weighted feedback from self, other hidden layer neurons, and output neurons. The hidden layer neuron weighted sum is expressed as:

$$HN(i) = \sum_{j=1}^{m} \mathcal{J}_j\omega_{ij}^I + \sum_{k=1}^{n} e\ell_H(i)\omega_{ik}^D + \sum_{l=1}^{r} e\ell_y(l)\omega_{il}^{OH} \tag{3.7}$$

Here $i = \{1, 2, \ldots, n\}, \omega^I \in R^{n\times m}, \omega^D \in R^{n\times n}$, and $\omega^{OH} \in R^{n\times r}$. $e\ell_{HN} = z^{-1}(HN) \in R^n$ is the feedback signal with single step delay. In this neural network (NN) algorithm sigmoid function is considered the activation function for the hidden layer output, expressed as follows:

$$\psi(i) = f_h\big(HN(i)\big) = \frac{1}{1 + e^{-HN(i)}}. \tag{3.8}$$

3) Output Layer in ECRNN: At the third layer of ECRNN, the output weights are calculated using the weighted sum of the output of the hidden layer. At this output layer, the linear activation function is considered. Therefore, ECRNN output is written as:

$$y = f_0\left(\varkappa^T \psi(\mathcal{J}, \omega^I, \omega^D, \omega^{OI}, \omega^{OH})\right) = \varkappa^T \psi. \quad 3.9$$

where the weights from neurons of the hidden layer to the neurons of the output layer are expressed as $\varkappa \in R^{n\times}$. The vector values of all weights are:

$\omega^I = vec(\omega_{ij}^I) \in R^{ij}\ with\ i = 1..m, j - 1..n,$

$\omega^D = vec(\omega_{ij}^D) \in R^{ij} with\ i = 1..n, j = 1..n.$

$\omega^{OI} = vec(\omega_{ij}^{OI}) \in R^{ij}\ with\ i = 1..r, j = 1..m.$

and

$\omega^{OH} = vec(\omega_{ij}^{OH}) \in R^{ij}\ with\ i = 1..r, j = 1..n$

As per the parameter set $G_\omega^I, G_\omega^D, G_\omega^{OI}\ and\ G_\omega^{OH}$ the Taylor series expansion is used to obtain the expression of $\tilde{\psi}$ in linearize form as:

$\tilde{\psi} = G_\omega^I \tilde{\omega}^I + G_\omega^D \tilde{\omega}^D + G_\omega^{OI} \tilde{\omega}^{OI} + G_\omega^{OH} \tilde{\omega}^{OH} + D_{ho}.$

Where, D_{ho} represents the higher-order derivative terms. These parametric values are given in a matrix form having diagonal vectors provided in eqns. (*3.10*)-(*3.13*), whereas other elements are zero in the matrix.

$$G_\omega^I = dig\{\psi_n(1-\psi_n)[I_{g1}\ I_{g2} \dots I_{gm}]\} \in R^{n\times mn} \quad 3.10$$

$$G_\omega^D = dig\{\psi_n(1-\psi_n)[E_{\ell 1}\ E_{\ell 2} \dots E_{\ell n}]\} \in R^{n\times nn} \quad 3.11$$

$$G_\omega^{OH} = dig\{\psi_n(1-\psi_n)[E_{y1}\ E_{y2} \dots E_{yr}]\} \in R^{n\times rn} \quad 3.12$$

$$G_\omega^{OI} = [\psi_n(1-\psi_n)[P_{\ell 1}\ P_{\ell 2} \dots P_{\ell r}]]^T \in R^{n\times rm} \quad 3.13$$

Where, $I_{gi} = \mathcal{J}_{gi} + \sum_{a=1}^{r} e\ell_y(a)\omega_{gia}^{OI}\ with\ i = 1..m, E_{\ell i} = e\ell_{HN}(i)\ with\ i = 1..n, E_{yi} = e\ell_y(i)\ with\ i = 1..r.$ and $P_{\ell i} = \sum_{l=1}^{m} e\ell_y(l)\omega_{gil}^I\ with\ i = 1..n.$ The ECRNN is a general neural network [55] configuration that follows the structure of radial basis NN (RBNN) [56], recurrent NN (RNN) [57], and backpropagation NN (BPNN) [58]. As if from the ECRNN, one feedback signal is taken from output to input or from output to the hidden layer, it will work as the BPNN. However, if only hidden layer feedback is considered, it will work as the RNN. The ECRNN [54] is more advantageous than feedforward NNs BPNN, RBNFN, RNN, and feedback NN as it has better approximation ability, excellent dynamic characteristics, and a stable structure compared

with its counter configurations.

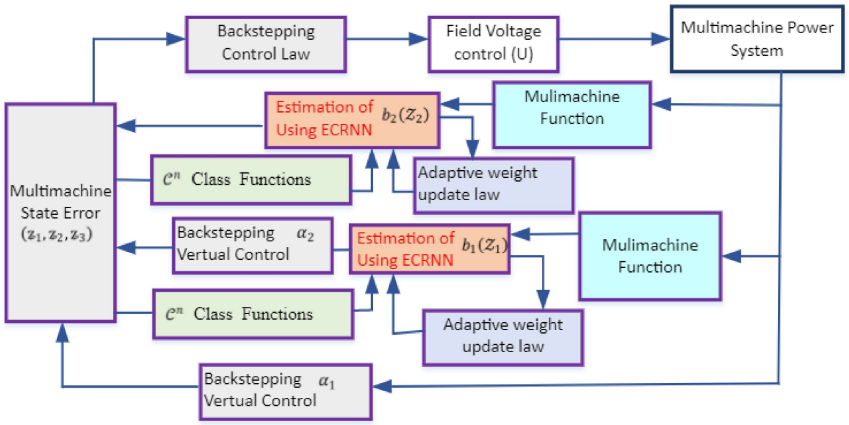

Figure 3.2. Block diagram of proposed Control Scheme.

3.3.1.3. Three $\mathcal{C}^n$-Class continuous functions.

The three continuous functions of $\mathcal{C}^n$-Class used to design the adaptive ECRNN-based backstepping control are defined as:

The first positive function of $\mathcal{C}^n$-Class is:

$$\mathcal{N}_{\mathfrak{c},n}(\mathfrak{z}) = \begin{cases} \dfrac{(|\mathfrak{z}| - \mathfrak{c})^n}{n!}, & |\mathfrak{z}| > \mathfrak{c} \\ 0, & |\mathfrak{z}| \leq \mathfrak{c} \end{cases} \tag{3.14}$$

With $\mathfrak{c}$ and n are the positive real and integer numbers.

$$sgn_{\mathfrak{c},n}(\mathfrak{z}) = \begin{cases} sgn(\mathfrak{z}), & |\mathfrak{z}| \geq \mathfrak{c} \\ 1 - 2cos^n\left(\dfrac{\pi}{2}sin^n\left(\dfrac{\pi}{4\mathfrak{c}}(\mathfrak{z} + \mathfrak{c})\right)\right), & |\mathfrak{z}| < \mathfrak{c} \end{cases} \tag{3.15}$$

The function $sign$ of $\mathcal{C}^n$-Class is expressed in eqn. (*3.15*). Now the third function is defined as:

$$p(\mathfrak{z}) = \begin{cases} 1, & |\mathfrak{z}| \leq \mathrm{F}_1 \\ cos^n\left(\dfrac{\pi}{2}sin^n\left(\dfrac{\pi}{2}\dfrac{|\mathfrak{z}|^2 - \mathrm{F}_1^2}{\mathrm{F}_2^2 - \mathrm{F}_1^2}\right)\right), & otherwise \\ 0, & |\mathfrak{z}| \geq \mathrm{F}_2 \end{cases} \tag{3.16}$$

Having F_1 & F_2 as the respective lower and upper bound of switching of $\mathfrak{z}$, whereas $\mathrm{F}_2 > \mathrm{F}_1 > 0$. Also,

$$M(\mathbb{Z}) := \prod_{i=1}^{m} p(\mathfrak{z}_i) \tag{3.17}$$

with $\mathbb{Z} = [z_1, \ldots, z_m]^T \in R^m$.

Lemma 3 presents the properties of three functions of $\mathcal{C}^n$-Class, $\mathcal{N}_{\epsilon,n}(z)$, $sgn_{\epsilon,n}(z)$, and $p(z)$.

Lemma 3: The properties of three functions $\mathcal{N}_{\epsilon,n}(z)$, $sgn_{\epsilon,n}(z)$, & $m(z)$ are:

1) $\mathcal{N}_{\epsilon,n+1}(z) \in \mathcal{C}^n$, $sgn_{\epsilon,n}(z) \in \mathcal{C}^n$, and $m(z) \in \mathcal{C}^n$. The function $\mathcal{N}_{\epsilon,n+1}(z)$ with q^{th}-order derivative,

$$\frac{d^q \mathcal{N}_{\epsilon,n+1}(z)}{dz^q} = \mathcal{N}_{\epsilon,n-q+1}(z)\left(sgn_{\epsilon,n-q+1}(z)\right)^q \tag{3.18}$$

Where $q = 1, \ldots, n$.

2) $\mathcal{N}_{\epsilon,n+1}(z)$ is a positive function, with the condition that if $|z| \leq \epsilon$, the function $\mathcal{N}_{\epsilon,n+1}(z) = 0$.

$$\frac{d\mathcal{N}_{\epsilon,n+1}(z)}{dz} sgn_{\epsilon,n}(z) = \mathcal{N}_{\epsilon,n}(z) \tag{3.19}$$

3.4 ECRNN Based Backstepping Excitation Control

The ECRNN algorithm estimates the associated control term to reduce the computational burden on the controller performance. Adaptive control laws are designed in a closed-loop network for unknown nonlinear dynamics [59]. The proposed backstepping scheme is applied to achieve the required objective of synchronous generator states stabilization as per eqns. (*2.1*)- (*2.3*) as give in chapter 1. In eqn. (*2.10*), the rotor angle of i^{th} the synchronous generator is expressed as δ_i.

Step 1: Now, the rotor angle deviation from the desired state is written as $z_1 = \delta_i - \delta_{id}$, where δ_{id} is the desired reference for the i^{th} synchronous generator. The derivative of z_1 is expressed as:

$$\dot{z}_1 = \dot{\delta}_i = \omega_i \tag{3.20}$$

In eqn. (*3.20*), ω_i represents the rotor speed. In backstepping scheme formulation, the second state error is written as:

$$z_2 = \omega_i - \omega_{id} \tag{3.21}$$

Here ω_{id} is the virtual input state. From the state error given in eqns. (*3.21*), (*3.22*) can be

written as:

$$\dot{z}_1 = z_2 + \omega_{id} \tag{3.22}$$

For the stability analysis at this stage $\dot{z}_1$ in terms of ω_{id} is required. The term ω_{id} is to be considered as virtual control input for another state analysis. As per Lyapunov stability criteria, the positive Lyapunov candidate is defined as:

$$\mathcal{V}_{z_1} = {}^1/_2\, z_1{}^2 \tag{3.23}$$

Here $\mathcal{V}_{z_1}$ is the strict positive Lyapunov candidate designed as per the state error z_1. The derivative of $\mathcal{V}_{z1}$, can be written as:

$$\dot{\mathcal{V}}_{z_1} = z_1 \omega_i \tag{3.24}$$

From the Lyapunov stability criteria, state stability is achieved if $\dot{\mathcal{V}}_{z1} \leq 0$. To reach this objective ω_{id} is designed as:

$$\omega_{id} = -k_1 z_1 \tag{3.25}$$

The value of k_1 is taken positive ($k_1 > 0$) as it is required to converge the state error z_1 so that the δ_{id} can be reached. Place the eqns. (*3.25*), in eqn. (*3.24*), Now, $\dot{\mathcal{V}}_{z1}$ can be written as:

$$\dot{\mathcal{V}}_{z_1} = -k_1 z_1{}^2 \tag{3.26}$$

Here it is observed that $\dot{\mathcal{V}}_{z1} \leq 0$. Thus, at this stage, the stability of the synchronous generator state is achieved.

Step 2: The second and third state error is defined as $z_2 = x_2 - \alpha_{1d}$ and $z_3 = x_3 - \alpha_{2d}$ respectively. Where α_{1d} is the virtual control input ω_{id}. Now Consider a nonnegative candidate as:

$$\begin{aligned}\mathcal{V}_{z_2} = \mathcal{V}_{z_1} + \frac{2!}{\theta_3 I_{qi}} \mathcal{N}_{\mathfrak{c},3}(z_2) + \frac{1}{2} \tilde{\varkappa}_1{}^T \Gamma_1{}^{-1} \tilde{\varkappa}_1 + \frac{1}{2\mu_1} \tilde{\Pi}_1{}^2 + \frac{1}{2\beth_1^I} \left(\tilde{\omega}_1{}^I\right)^T \tilde{\omega}_1{}^I \\ + \frac{1}{2\beth_1^D} \left(\tilde{\omega}_1{}^D\right)^T \tilde{\omega}_1{}^D + \frac{1}{2\beth_1^{OI}} \left(\tilde{\omega}_1{}^{OI}\right)^T \tilde{\omega}_1{}^{OI} + \frac{1}{2\beth_1^{OH}} \left(\tilde{\omega}_1{}^{OH}\right)^T \tilde{\omega}_1{}^{OH} \\ + \frac{1}{2\beth_1^{\Delta_{g1}}} \left(\tilde{\Delta}_{g1}\right)^T \tilde{\Delta}_{g1}\end{aligned} \tag{3.27}$$

Taking the derivative of $\mathcal{V}_{z_2}$ for the system stability with $\mathfrak{g}_1 = \theta_3 I_{qi}$ and $f_1(x_2) = \theta_1 x_2 + \theta_2$.

$$\dot{\mathcal{V}}_{z_2} = -k_1 z_1{}^2 + \frac{2}{g_1}\frac{d\mathcal{N}_{\epsilon,3}(z_2)}{dz_2}\dot{z}_2 - \frac{2\dot{g}_1}{g_1{}^2}\mathcal{N}_{\epsilon,3}(z_2) - \tilde{\varkappa}_1{}^T \Gamma_1{}^{-1}\dot{\hat{\varkappa}}_1 - \frac{1}{\mu_1}\tilde{\eta}_1\dot{\hat{\eta}}_1 - \frac{1}{\beta_1^I}\left(\tilde{\omega}_1{}^I\right)^T\dot{\hat{\omega}}_1{}^I - \frac{1}{\beta_1^D}\left(\tilde{\omega}_1{}^D\right)^T\dot{\hat{\omega}}_1{}^D - \frac{1}{\beta_1^{OI}}\left(\tilde{\omega}_1{}^{OI}\right)^T\dot{\hat{\omega}}_1{}^{OI} - \frac{1}{\beta_1^{OH}}\left(\tilde{\omega}_1{}^{OH}\right)^T\dot{\hat{\omega}}_1{}^{OH} - \frac{1}{\beta_1^{\Delta_{g1}}}\left(\tilde{\Delta}_{g1}\right)^T\dot{\hat{\Delta}}_{g1} \quad 3.28$$

$$\dot{\mathcal{V}}_{z_2} = -k_1 z_1{}^2 + 2\frac{d\mathcal{N}_{\epsilon,3}(z_2)}{dz_2}\left[\frac{f_1(\bar{x}_2) - \dot{\alpha}_{1d}}{g_1} + z_3 + \alpha_{2d} - \dot{g}_1\mathfrak{T}_1(\mathcal{Z}_1)\right] - \tilde{\varkappa}_1{}^T\Gamma_1{}^{-1}\dot{\hat{\varkappa}}_1 - \frac{1}{\mu_1}\tilde{\eta}_1\dot{\hat{\eta}}_1 - \frac{1}{\beta_1^I}\left(\tilde{\omega}_1{}^I\right)^T\dot{\hat{\omega}}_1{}^I - \frac{1}{\beta_1^D}\left(\tilde{\omega}_1{}^D\right)^T\dot{\hat{\omega}}_1{}^D - \frac{1}{\beta_1^{OI}}\left(\tilde{\omega}_1{}^{OI}\right)^T\dot{\hat{\omega}}_1{}^{OI} - \frac{1}{\beta_1^{OH}}\left(\tilde{\omega}_1{}^{OH}\right)^T\dot{\hat{\omega}}_1{}^{OH} - \frac{1}{\beta_1^{\Delta_{g1}}}\left(\tilde{\Delta}_{g1}\right)^T\dot{\hat{\Delta}}_{g1} \quad 3.29$$

$$\mathfrak{T}_1(\mathcal{Z}_1) = \begin{cases}\left[\dfrac{d\mathcal{N}_{\epsilon,3}(z_2)}{dz_2}\right]^{-1}\dfrac{\mathcal{N}_{\epsilon,3}(z_2)}{g_1{}^2}, & |z_2| > \epsilon \\ 0, & |z_2| \le \epsilon\end{cases} \quad 3.30$$

with $\mathcal{Z}_1 = \left[x_2, \alpha_{1d}, \frac{d\alpha_{1d}}{dx_1}\right]^T \in R^3$ and $\mathbb{Q}_{z_2} \subseteq R^3$. Function $b_1(\mathcal{Z}_1)$ is continuous. Therefore, this function is approximated with $\mathcal{Z}_1 \in \mathbb{Q}_{z_2}$ by the ECRNN algorithm as:

$$b_1(\mathcal{Z}_1) = \varkappa_1{}^T\psi_1(\mathcal{Z}_1) + \mathfrak{E}_1(\mathcal{Z}_1) \quad 3.31$$

The approximation error is $\mathfrak{E}_1(\mathcal{Z}_1)$, satisfying the inequality $|\mathfrak{E}_1(\mathcal{Z}_1)| \le \mathfrak{p}_1$, where $\mathfrak{p}_1 > 0$. Additionally, a positive function $\beta_1(\mathcal{Z}_1)$ and a constant η_1 is exist such that [52]:

$$|b_1(\mathcal{Z}_1)| \le \eta_1\beta_1(\mathcal{Z}_1) \quad 3.32$$

$$\dot{\mathcal{V}}_{z_2} = -k_1 z_1{}^2 + 2\frac{d\mathcal{N}_{\epsilon,3}(z_2)}{dz_2}[b_1(\mathcal{Z}_1) + z_3 + \alpha_{2d}] - \tilde{\varkappa}_1{}^T\Gamma_1{}^{-1}\dot{\hat{\varkappa}}_1 - \frac{1}{\mu_1}\tilde{\eta}_1\dot{\hat{\eta}}_1 - \frac{1}{\beta_1^I}\left(\tilde{\omega}_1{}^I\right)^T\dot{\hat{\omega}}_1{}^I - \frac{1}{\beta_1^D}\left(\tilde{\omega}_1{}^D\right)^T\dot{\hat{\omega}}_1{}^D - \frac{1}{\beta_1^{OI}}\left(\tilde{\omega}_1{}^{OI}\right)^T\dot{\hat{\omega}}_1{}^{OI} - \frac{1}{\beta_1^{OH}}\left(\tilde{\omega}_1{}^{OH}\right)^T\dot{\hat{\omega}}_1{}^{OH} - \frac{1}{\beta_1^{\Delta_{g1}}}\left(\tilde{\Delta}_{g1}\right)^T\dot{\hat{\Delta}}_{g1} \quad 3.33$$

$$\dot{\mathcal{V}}_{z_2} = -k_1 z_1{}^2 + 2\frac{d\mathcal{N}_{\epsilon,3}(z_2)}{dz_2}\{M(\mathbb{Z}_1)\,[\varkappa_1{}^T\psi_1(\mathcal{Z}_1) + \mathfrak{E}_1(\mathcal{Z}_1)] + [1 - M(\mathbb{Z}_1)]b_1(\mathcal{Z}_1) + z_3 + \alpha_{2d}\} - \tilde{\varkappa}_1{}^T\Gamma_1{}^{-1}\dot{\hat{\varkappa}}_1 - \frac{1}{\mu_1}\tilde{\eta}_1\dot{\hat{\eta}}_1 - \frac{1}{\beta_1^I}\left(\tilde{\omega}_1{}^I\right)^T\dot{\hat{\omega}}_1{}^I - \frac{1}{\beta_1^D}\left(\tilde{\omega}_1{}^D\right)^T\dot{\hat{\omega}}_1{}^D - \frac{1}{\beta_1^{OI}}\left(\tilde{\omega}_1{}^{OI}\right)^T\dot{\hat{\omega}}_1{}^{OI} - \frac{1}{\beta_1^{OH}}\left(\tilde{\omega}_1{}^{OH}\right)^T\dot{\hat{\omega}}_1{}^{OH} - \frac{1}{\beta_1^{\Delta_{g1}}}\left(\tilde{\Delta}_{g1}\right)^T\dot{\hat{\Delta}}_{g1} \quad 3.34$$

Here the $\dot{\mathcal{V}}_{z_2}$ is obtained in eqn (*3.33*). The inequality $|f(x)| = f(x)sign\big(f(x)\big)$ is useful for further analysis. From this inequality and eqn. (*3.19*) the $\dot{\mathcal{V}}_{z_2}$ can be modified as:

$$\begin{aligned}\dot{\mathcal{V}}_{z_2} \leq -k_1 z_1{}^2 + 2\mathcal{N}_{c,2}(z_2)sgn_{c,2}(z_2)\{M(\mathbb{Z}_1)\,[\varkappa_1{}^T\psi_1(\mathcal{Z}_1) + \mathrm{p}_1] \\ + [1 - M(\mathbb{Z}_1)]\eta_1\beta_1(\mathcal{Z}_1)sgn_{c,2}(z_2) + z_3 + \alpha_{2d}\} - \tilde{\varkappa}_1{}^T\Gamma_1{}^{-1}\dot{\hat{\varkappa}}_1 \\ -\frac{1}{\mu_1}\tilde{\eta}_1\dot{\hat{\eta}}_1 - \frac{1}{\beth_1^I}\big(\tilde{\omega}_1{}^I\big)^T\dot{\hat{\omega}}_1{}^I - \frac{1}{\beth_1^D}\big(\tilde{\omega}_1{}^D\big)^T\dot{\hat{\omega}}_1{}^D - \frac{1}{\beth_1^{OI}}\big(\tilde{\omega}_1{}^{OI}\big)^T\dot{\hat{\omega}}_1{}^{OI} \\ -\frac{1}{\beth_1^{OH}}\big(\tilde{\omega}_1{}^{OH}\big)^T\dot{\hat{\omega}}_1{}^{OH} - \frac{1}{\beth_1^{\Delta_{g1}}}\big(\tilde{\Delta}_{g1}\big)^T\dot{\hat{\Delta}}_{g1}\end{aligned} \tag{3.35}$$

from the above equation, the virtual input α_{2d} can be written as:

$$\begin{aligned}\alpha_{2d} = -2C_1\mathcal{N}_{c,2}(z_2)sgn_{c,2}(z_2) - M(\mathbb{Z}_1)\left[\hat{\varkappa}_1{}^T\hat{\psi}_1(\mathcal{Z}_1)\right] \\ - [1 - M(\mathbb{Z}_1)]\hat{\eta}_1\beta_1(\mathcal{Z}_1)sgn_{c,2}(z_2) - (c+1)sgn_{c,2}(z_2)\end{aligned} \tag{3.36}$$

The error of a function is defined $\tilde{*} = * - \hat{*}$, with $\hat{*}$ is the estimate of $*$. Form this, it can be written as:

$$\begin{aligned}\varkappa_1{}^T\psi_1(\mathcal{Z}_1) + \mathrm{p}_1 - \hat{\varkappa}_1{}^T\hat{\psi}_1(\mathcal{Z}_1) \\ = \big[\hat{\varkappa}_1{}^T\big(G_\omega^I\tilde{\omega}_1{}^I + G_\omega^D\tilde{\omega}_1{}^D + G_\omega^{OI}\tilde{\omega}_1{}^{OI} + G_\omega^{OH}\tilde{\omega}_1{}^{OH}\big) \\ + \tilde{\varkappa}_1{}^T\big(\hat{\psi}_1 + G_\omega^I\tilde{\omega}_1{}^I + G_\omega^D\tilde{\omega}_1{}^D + G_\omega^{OI}\tilde{\omega}_1{}^{OI} + G_\omega^{OH}\tilde{\omega}_1{}^{OH}\big) + \varkappa_1{}^T D_{ho} \\ + \mathrm{p}_1\big]\end{aligned} \tag{3.37}$$

$$\begin{aligned}\varkappa_1{}^T\psi_1(\mathcal{Z}_1) + \mathrm{p}_1 - \hat{\varkappa}_1{}^T\hat{\psi}_1(\mathcal{Z}_1) \\ = \big[\hat{\varkappa}_1{}^T\big(G_\omega^I\tilde{\omega}_1{}^I + G_\omega^D\tilde{\omega}_1{}^D + G_\omega^{OI}\tilde{\omega}_1{}^{OI} + G_\omega^{OH}\tilde{\omega}_1{}^{OH}\big) \\ + \tilde{\varkappa}_1{}^T\big(\hat{\psi}_1 - G_\omega^I\hat{\omega}_1{}^I - G_\omega^D\hat{\omega}_1{}^D - G_\omega^{OI}\hat{\omega}_1{}^{OI} - G_\omega^{OH}\hat{\omega}_1{}^{OH}\big) + \Delta_{g1}\big]\end{aligned} \tag{3.38}$$

$\Delta_1 = \tilde{\varkappa}_1{}^T(G_\omega^I\omega_1{}^I + G_\omega^D\omega_1{}^D + G_\omega^{OI}\omega_1{}^{OI} + G_\omega^{OH}\omega_1{}^{OH} + D_{ho}) + \mathrm{p}_1$ is an overall estimation error. It has ideal weights as well as an approximation error of ECRNN. Practically perfect weights are unknown, so they are included in Δ. Assuming Δ to be bounded as $\big(|\Delta_1| < \Delta_{g1}\big)$. Here Δ_{g1} is estimated through the adaptive law for the compensation of approximation error of ECRNN during $b_1(\mathcal{Z}_1)$ estimation. Now from eqns. (*3.30*) and (*3.38*), the adaptive laws are obtained as:

$$\begin{aligned}\dot{\hat{\varkappa}}_1 = 2\Gamma_1\mathcal{N}_{c,2}(z_2)sgn_{c,2}(z_2)M(\mathbb{Z}_1)\big(\hat{\psi}_1 - G_\omega^I\hat{\omega}_1{}^I - G_\omega^D\hat{\omega}_1{}^D - G_\omega^{OI}\hat{\omega}_1{}^{OI} \\ - G_\omega^{OH}\hat{\omega}_1{}^{OH}\big)\end{aligned} \tag{3.39}$$

$$\dot{\hat{\eta}}_1 = 2\mu_1\mathcal{N}_{c,2}(z_2)[1 - M(\mathbb{Z}_1)]\beta_1(\mathcal{Z}_1) \tag{3.40}$$

$$\dot{\hat{\omega}}_1{}^{\xi} = 2\beth_1^{\xi}\mathcal{N}_{c,2}(z_2)sgn_{c,2}(z_2)M(\mathbb{Z}_1)\hat{\varkappa}_1{}^T G_\omega^{\xi} \tag{3.41}$$

with $\xi = I, D, OI\ and\ OH$.

$$\dot{\hat{\Delta}}_{g1} = 2\beth_1^{\Delta_{g1}} \mathcal{N}_{\mathfrak{c},2}(\mathfrak{z}_2) sgn_{\mathfrak{c},2}(\mathfrak{z}_2) M(\mathbb{Z}_1) \tag{3.42}$$

Now, $\dot{\mathcal{V}}_{\mathfrak{z}_2}$ can be obtained as:

$$\begin{aligned}\dot{\mathcal{V}}_{\mathfrak{z}_2} \leq -k_1 {\mathfrak{z}_1}^2 - 4C_1 {\mathcal{N}_{\mathfrak{c},2}}^2(\mathfrak{z}_2) - 2\beth_1^{\Delta_{g1}} \mathcal{N}_{\mathfrak{c},2}(\mathfrak{z}_2) sgn_{\mathfrak{c},2}(\mathfrak{z}_2) M(\mathbb{Z}_1)\hat{\Delta}_{g1} \\ + 2\mathcal{N}_{\mathfrak{c},2}(\mathfrak{z}_2)[|\mathfrak{z}_3| - (\mathfrak{c}+1)]\end{aligned} \tag{3.43}$$

Step 3: The derivative of the third state error can be expressed as $\dot{\mathfrak{z}}_3 = f_2(x_3) + \mathfrak{g}_2 U - \dot{\alpha}_{2d}$ with $f_2(x_3) = -\theta_4 x_3 + \theta_5 I_{di}$ and $\mathfrak{g}_2 = \theta_4$. Where α_{2d} is considered as the third virtual control input. The derivative of α_{2d} can be expressed as:

$$\begin{aligned}\dot{\alpha}_{2d} = \frac{d\alpha_{2d}}{dx_1}[x_2] + \frac{d\alpha_{2d}}{dx_2}[f_1(x_2) + \mathfrak{g}_1 x_3] + \frac{d\alpha_{2d}}{d\hat{\varkappa}_2}\dot{\hat{\varkappa}}_2 + \frac{d\alpha_{2d}}{d\hat{\omega}_2{}^I}\dot{\hat{\omega}}_2{}^I + \frac{d\alpha_{2d}}{d\hat{\omega}_2{}^D}\dot{\hat{\omega}}_2{}^D \\ + \frac{d\alpha_{2d}}{d\hat{\omega}_2{}^{OI}}\dot{\hat{\omega}}_2{}^{OI} + \frac{d\alpha_{2d}}{d\hat{\omega}_2{}^{OH}}\dot{\hat{\omega}}_2{}^{OH} + \frac{d\alpha_{2d}}{d\hat{\Pi}_2}\dot{\hat{\Pi}}_2 + \frac{d\alpha_{2d}}{d\hat{\Delta}_{g1}}\dot{\hat{\Delta}}_{g1}\end{aligned} \tag{3.44}$$

Now let us take a nonnegative candidate $\mathcal{V}_{\mathfrak{z}_3}$ as:

$$\begin{aligned}\mathcal{V}_{\mathfrak{z}_3} = \mathcal{V}_{\mathfrak{z}_2} + \frac{\mathcal{N}_{\mathfrak{c},2}(\mathfrak{z}_3)}{\mathfrak{g}_2} + \frac{1}{2}\tilde{\varkappa}_2{}^T \Gamma_2{}^{-1}\tilde{\varkappa}_2 + \frac{1}{2\mu_2}\tilde{\Pi}_2{}^2 + \frac{1}{2\beth_2^I}\left(\tilde{\omega}_2{}^I\right)^T\tilde{\omega}_2{}^I \\ + \frac{1}{2\beth_2^D}\left(\tilde{\omega}_2{}^D\right)^T\tilde{\omega}_2{}^D + \frac{1}{2\beth_2^{OI}}\left(\tilde{\omega}_2{}^{OI}\right)^T\tilde{\omega}_2{}^{OI} + \frac{1}{2\beth_2^{OH}}\left(\tilde{\omega}_2{}^{OH}\right)^T\tilde{\omega}_2{}^{OH} \\ + \frac{1}{2\beth_2^{\Delta_{g2}}}\left(\tilde{\Delta}_{g2}\right)^T\tilde{\Delta}_{g2}\end{aligned} \tag{3.45}$$

Taking the derivative of $\mathcal{V}_{\mathfrak{z}_3}$ for the system stability as:

$$\begin{aligned}\dot{\mathcal{V}}_{\mathfrak{z}_3} = \dot{\mathcal{V}}_{\mathfrak{z}_2} + \frac{d\mathcal{N}_{\mathfrak{c},2}(\mathfrak{z}_3)}{d\mathfrak{z}_3}\left[\frac{f_2(\bar{x}_3) - \dot{\alpha}_{2d}}{\mathfrak{g}_2} + U - \dot{\mathfrak{g}}_2\mathfrak{T}_2(\mathcal{Z}_2)\right] - \tilde{\varkappa}_2{}^T\Gamma_2{}^{-1}\dot{\hat{\varkappa}}_2 - \frac{1}{\mu_1}\tilde{\Pi}_2\dot{\hat{\Pi}}_2 \\ - \frac{1}{\beth_2^I}\left(\tilde{\omega}_2{}^I\right)^T\dot{\hat{\omega}}_2{}^I - \frac{1}{\beth_2^D}\left(\tilde{\omega}_2{}^D\right)^T\dot{\hat{\omega}}_2{}^D - \frac{1}{\beth_2^{OI}}\left(\tilde{\omega}_2{}^{OI}\right)^T\dot{\hat{\omega}}_2{}^{OI} \\ - \frac{1}{\beth_2^{OH}}\left(\tilde{\omega}_2{}^{OH}\right)^T\dot{\hat{\omega}}_2{}^{OH} - \frac{1}{\beth_2^{\Delta_{g2}}}\left(\tilde{\Delta}_{g2}\right)^T\dot{\hat{\Delta}}_{g2}\end{aligned} \tag{3.46}$$

$$\mathfrak{T}_2(\mathcal{Z}_2) = \begin{cases}\left[\frac{d\mathcal{N}_{\mathfrak{c},3}(\mathfrak{z}_3)}{d\mathfrak{z}_3}\right]^{-1}\frac{\mathcal{N}_{\mathfrak{c},2}(\mathfrak{z}_3)}{{\mathfrak{g}_2}^2}, & |\mathfrak{z}_3| > \mathfrak{c} \\ 0, & |\mathfrak{z}_3| \leq \mathfrak{c}\end{cases} \tag{3.47}$$

with $\mathcal{Z}_2 = \left[x_3, \alpha_{2d}, \frac{d\alpha_{2d}}{dx_1}, \frac{d\alpha_{2d}}{dx_2}\right]^T \in R^4$. Chosen a compact vector set as $\mathfrak{Q}_{\mathfrak{z}_3} \subseteq R^3$. The function $b_2(\mathcal{Z}_2)$ is continuous. Therefore, this function is approximated with $\mathcal{Z}_2 \in \mathfrak{Q}_{\mathfrak{z}_3}$ through the ECRNN algorithm as:

$$b_2(\mathcal{Z}_2) = \varkappa_2{}^T\psi_2(\mathcal{Z}_2) + \mathfrak{E}_2(\mathcal{Z}_2) \tag{3.48}$$

The approximation error is $\Sigma_2(\mathcal{Z}_2)$, satisfying the inequality $|\Sigma_2(\mathcal{Z}_2)| \leq \rho_2$, where $\rho_2 > 0$. Additionally, a positive function $\beta_2(\mathcal{Z}_2)$ and a constant η_2 is exist such that [52]:

$$|b_2(\mathcal{Z}_2)| \leq \eta_2 \beta_2(\mathcal{Z}_2) \tag{3.49}$$

Now the $\dot{\mathcal{V}}_{z_2}$ can be written as:

$$\begin{aligned}\dot{\mathcal{V}}_{z_2} = \dot{\mathcal{V}}_{z_2} + \frac{d\mathcal{N}_{c,2}(z_3)}{dz_3}[b_1(\mathcal{Z}_1) + U] - \tilde{\varkappa}_2{}^T \Gamma_2{}^{-1}\dot{\hat{\varkappa}}_2 - \frac{1}{\mu_2}\tilde{\eta}_2\dot{\hat{\eta}}_2 - \frac{1}{\beta_2^I}\left(\tilde{\omega}_2{}^I\right)^T \dot{\hat{\omega}}_2{}^I \\ - \frac{1}{\beta_2^D}\left(\tilde{\omega}_2{}^D\right)^T \dot{\hat{\omega}}_2{}^D - \frac{1}{\beta_2^{OI}}\left(\tilde{\omega}_2{}^{OI}\right)^T \dot{\hat{\omega}}_2{}^{OI} - \frac{1}{\beta_2^{OH}}\left(\tilde{\omega}_2{}^{OH}\right)^T \dot{\hat{\omega}}_2{}^{OH} \\ - \frac{1}{\beta_2^{\Delta_{g2}}}\left(\tilde{\Delta}_{g2}\right)^T \dot{\hat{\Delta}}_{g2}\end{aligned} \tag{3.50}$$

$$\begin{aligned}\dot{\mathcal{V}}_{z_2} = \dot{\mathcal{V}}_{z_2} + \frac{d\mathcal{N}_{c,2}(z_3)}{dz_3}\{M(\mathbb{Z}_2)\,[\varkappa_2{}^T\psi_2(\mathcal{Z}_2) + \Sigma_2(\mathcal{Z}_2)] + [1 - M(\mathbb{Z}_2)]b_2(\mathcal{Z}_2) \\ + U\} - \tilde{\varkappa}_2{}^T \Gamma_2{}^{-1}\dot{\hat{\varkappa}}_2 - \frac{1}{\mu_2}\tilde{\eta}_2\dot{\hat{\eta}}_2 - \frac{1}{\beta_2^I}\left(\tilde{\omega}_2{}^I\right)^T \dot{\hat{\omega}}_2{}^I - \frac{1}{\beta_2^D}\left(\tilde{\omega}_2{}^D\right)^T \dot{\hat{\omega}}_2{}^D \\ - \frac{1}{\beta_2^{OI}}\left(\tilde{\omega}_2{}^{OI}\right)^T \dot{\hat{\omega}}_2{}^{OI} - \frac{1}{\beta_2^{OH}}\left(\tilde{\omega}_2{}^{OH}\right)^T \dot{\hat{\omega}}_2{}^{OH} - \frac{1}{\beta_2^{\Delta_{g2}}}\left(\tilde{\Delta}_{g2}\right)^T \dot{\hat{\Delta}}_{g2}\end{aligned} \tag{3.51}$$

$$\begin{aligned}\dot{\mathcal{V}}_{z_3} \leq \dot{\mathcal{V}}_{z_2} + \mathcal{N}_{c,1}(z_3)sgn_{c,1}(z_3)\{M(\mathbb{Z}_2)\,[\varkappa_3{}^T\psi_3(\mathcal{Z}_3) + \rho_3] \\ + [1 - M(\mathbb{Z}_2)]\eta_2\beta_2(\mathcal{Z}_2)sgn_{c,2}(z_3) + U\} - \tilde{\varkappa}_2{}^T \Gamma_2{}^{-1}\dot{\hat{\varkappa}}_2 - \frac{1}{\mu_2}\tilde{\eta}_2\dot{\hat{\eta}}_2 \\ - \frac{1}{\beta_2^I}\left(\tilde{\omega}_2{}^I\right)^T \dot{\hat{\omega}}_2{}^I - \frac{1}{\beta_2^D}\left(\tilde{\omega}_2{}^D\right)^T \dot{\hat{\omega}}_2{}^D - \frac{1}{\beta_2^{OI}}\left(\tilde{\omega}_2{}^{OI}\right)^T \dot{\hat{\omega}}_2{}^{OI} \\ - \frac{1}{\beta_2^{OH}}\left(\tilde{\omega}_2{}^{OH}\right)^T \dot{\hat{\omega}}_2{}^{OH} - \frac{1}{\beta_2^{\Delta_{g2}}}\left(\tilde{\Delta}_{g2}\right)^T \dot{\hat{\Delta}}_{g2}\end{aligned} \tag{3.52}$$

$$\begin{aligned}U = -C_2\mathcal{N}_{c,1}(z_3)sgn_{c,1}(z_3) - M(\mathbb{Z}_2)\left[\hat{\varkappa}_2{}^T\hat{\psi}_2(\mathcal{Z}_2)\right] \\ - [1 - M(\mathbb{Z}_2)]\hat{\eta}_2\beta_2(\mathcal{Z}_2)sgn_{c,1}(z_3)\end{aligned} \tag{3.53}$$

Now from eqns. (*3.52*) and (*3.53*), the adaptive laws for

$\varkappa_2, \omega_2{}^I, \omega_2{}^D, \omega_2{}^{OI}, \omega_2{}^{OH}, \Delta_{g2}\ and\ \eta_2$ can be designed as:

$$\begin{aligned}\dot{\hat{\varkappa}}_2 = \Gamma_2\mathcal{N}_{c,1}(z_3)sgn_{c,2}(z_3)M(\mathbb{Z}_2)\big(\hat{\psi}_2 - G_\omega^I\hat{\omega}_2{}^I - G_\omega^D\hat{\omega}_2{}^D - G_\omega^{OI}\hat{\omega}_2{}^{OI} \\ - G_\omega^{OH}\hat{\omega}_2{}^{OH}\big)\end{aligned} \tag{3.54}$$

$$\dot{\hat{\eta}}_2 = \mu_2\mathcal{N}_{c,1}(z_2)[1 - M(\mathbb{Z}_2)]\beta_2(\mathcal{Z}_2) \tag{3.55}$$

$$\dot{\hat{\omega}}_2{}^{\delta} = \beta_2^{\delta}\mathcal{N}_{c,1}(z_3)sgn_{c,1}(z_3)M(\mathbb{Z}_2)\hat{\varkappa}_2{}^T G_\omega^{\delta} \tag{3.56}$$

with $\delta = I, D, OI\ and\ OH$

$$\dot{\hat{\Delta}}_{g2} = \beta_2^{\Delta_{g2}}\mathcal{N}_{c,1}(z_3)sgn_{c,1}(z_3)M(\mathbb{Z}_2) \tag{3.57}$$

And the $\dot{\mathcal{V}}_{z_3}$ can be obtained as:

$$\dot{\mathcal{V}}_{z_3} \leq \dot{\mathcal{V}}_{z_2} - C_2 \mathcal{N}_{\mathfrak{c},1}{}^2(z_3) - 2\beth_2^{\Delta_{g2}} \mathcal{N}_{\mathfrak{c},1}(z_3) sgn_{\mathfrak{c},1}(z_3) M(\mathbb{Z}_2) \hat{\Delta}_{g2} \tag{3.58}$$

$$\begin{aligned} \dot{\mathcal{V}}_{z_3} \leq & -k_1 z_1{}^2 - 4C_1 \mathcal{N}_{\mathfrak{c},2}{}^2(z_2) - C_2 \mathcal{N}_{\mathfrak{c},1}{}^2(z_3) \\ & - 2\beth_1^{\Delta_{g1}} \mathcal{N}_{\mathfrak{c},2}(z_2) sgn_{\mathfrak{c},2}(z_2) M(\mathbb{Z}_1) \hat{\Delta}_{g1} \\ & - 2\beth_2^{\Delta_{g2}} \mathcal{N}_{\mathfrak{c},1}(z_3) sgn_{\mathfrak{c},1}(z_3) M(\mathbb{Z}_2) \hat{\Delta}_{g2} + \mathcal{N}_{\mathfrak{c},2}(z_2)[|z_3| - (\mathfrak{c}+1)] \end{aligned} \tag{3.59}$$

For the bounded initial values, the adaptive closed-loop power system has dynamics given in eqns. (*3.1*)-(*3.3*), with the virtual variables in eqns. (*3.25*) & (*3.36*), control law in eqn. (*3.53*) and adaptive laws provided in eqns. (*3.39*)-(*3.42*) & eqns. (*3.54*)-(*3.57*), and stability of the closed-loop system is ensured provided that all closed-loop variables:

$x_i, \alpha_i, U,\ \hat{\varkappa}_i, \omega_i{}^I, \omega_i{}^D, \omega_i{}^{OI}, \omega_i{}^{OH}, \Delta_{\mathrm{gi}}$ & η_{i} $with\ 1 = 1{,}2$ are remained bounded, and the state errors z_i follows $|z_i(t)| \leq \mathfrak{c}$ for $t \to \infty$, or $|x_i - \alpha_{(i-1)d}| \leq \mathfrak{c}$ for $t \to \infty$.

3.5 Verification and Simulation of Proposed Scheme

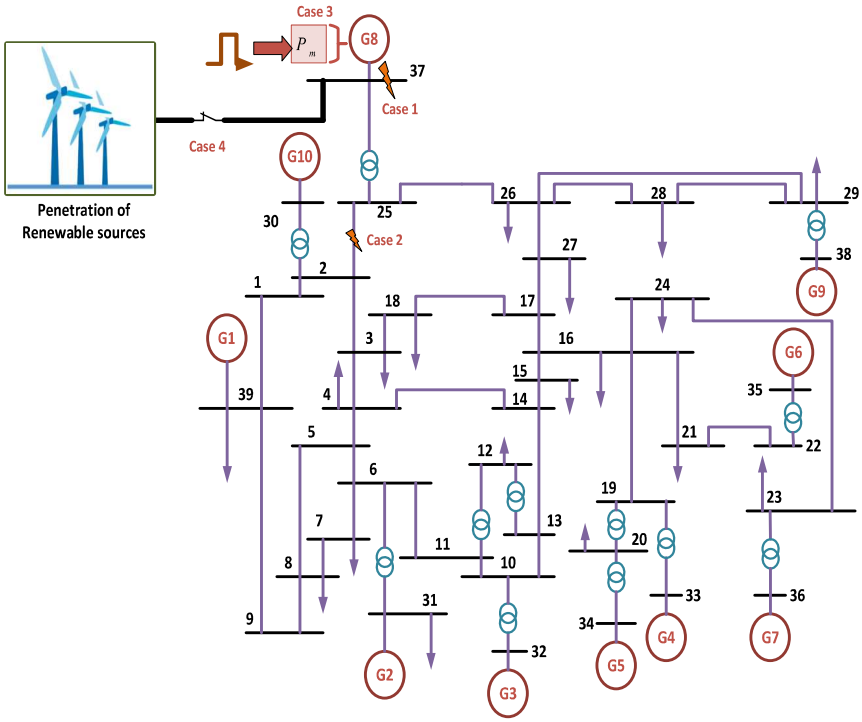

Figure 3.3. IEEE 39 Bus, 10-Machine new England Power System.

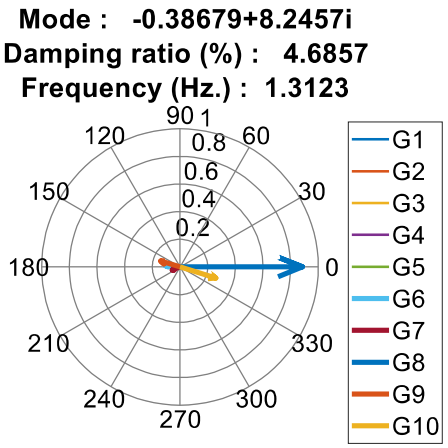

Figure 3.4. Compass plot of base system network of IEEE 39 bus system.

Power System Specifications and Parameters

Parameters	Value
$E_f(pu)$	1.90805
$E_{\min\_max}(pu)$	± 5,
$V_T(pu)$	$1.03V$
H	$2.43sec$
$x'_d(pu)$	0.57
$x_d(pu)$	2.9
T'_{do}	$0.003sec$
T_{do}	$6.7sec$
$R_{G8}(pu)$ and $X_{G8}(pu)$	$0.00686, 0.280$
$R_{B25-B26}$ and $X_{B25-B26}$	$0.0032, 0.0323$
Proposed controller gains	$k_1 = 1.223, \mathrm{p}_1 = 0.23, \mathrm{p}_2 = 0.84, C_1 = C_2 = 0.35,$
Controller parameters [38] and [41]	$c_1 = c_2 = c_3 = 2, \gamma = 2, \rho = 4, \alpha = 0.1, \alpha_1 = \beta_1 = \alpha_2 = \beta_2 = \alpha_3 = \beta_3 = \alpha_4 = \beta_4 = 0.2, \tau_1 = \tau_2 = 0.2$

Table 3.1. Power System Specifications and Parameters

The verification of the proposed control scheme is carried out in the MATLAB/Simulink platform. The simulation of the IEEE 39-bus, 10-machines New England power system model shown in Figure *3.2* is simulated as per the specifications given in Table 3.1. The other corresponding system parameters detail is taken from [16]. The IEEE 39 bus model in the power system exhibits ten synchronous generators with a power generation of 6193.41 MW and incorporates static & dynamic loads with a demand

of 6150.5 MW Load. Each exciter's voltage limit is considered as $\pm 5\, pu$ to avoid overvoltage problems. The model shown in Figure *3.3*is the excitation system of IEEE ST1 exciter, also known as IEEE type II.

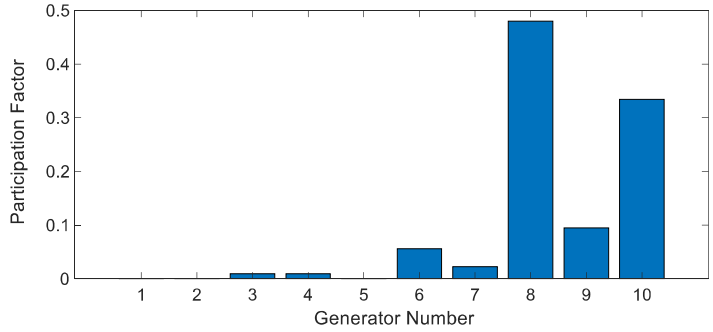

Figure 3.5. Participation factors of ten generators in the power system network.

Two-axis model of a synchronous generator is considered as generator nodes. As per the modal analysis [16] at the base value condition, the compass plot and participation factor of the generators to least damped mode 1.3123 Hz are respectively shown in Figure *3.4* and Figure *3.5*. As depicted in Figure *3.4*, the generator $G8$ oscillates against the generator $G6$, and it is seen that the generator $G8$ has the highest participation factor in this mode. Therefore, generator $G8$ which is connected to bus-37 is selected for employment of the proposed control scheme. For evaluation of the controller performance following cases are performed in the simulation study.

- *Case 1:* A three-phase short circuit fault at the terminal of generator $G8$ is applied at $t = 30\ sec$ for $0.2\ sec$ duration.
- *Case 2:* A three-phase short circuit fault at the transmission line between bus-25 and bus-2 is applied at $t = 30\ sec$ for $0.2\ sec$.
- *Case 3:* The mechanical power input is increased by 5% to analyze the transient efficacy of the proposed scheme applied at $G8$.
- *Case 4:* A wind farm renewable power source of $210\ MW$ capacity is integrated into bus 37 at $t = 0\ sec$, and it is detached from the system at $t = 30\ sec$.

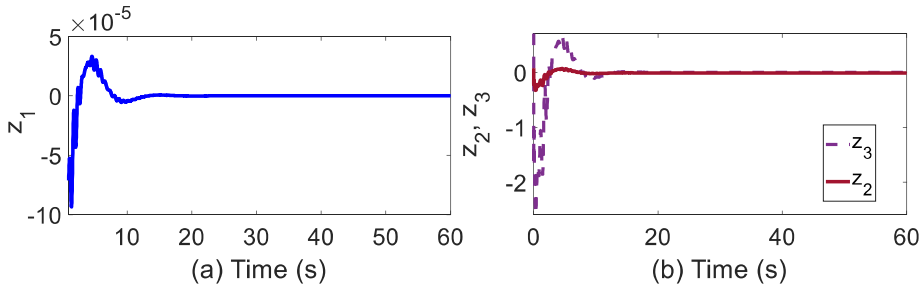

Figure 3.6. Generator G_8 state errors response (a) z_1 (b) z_2 and z_3.

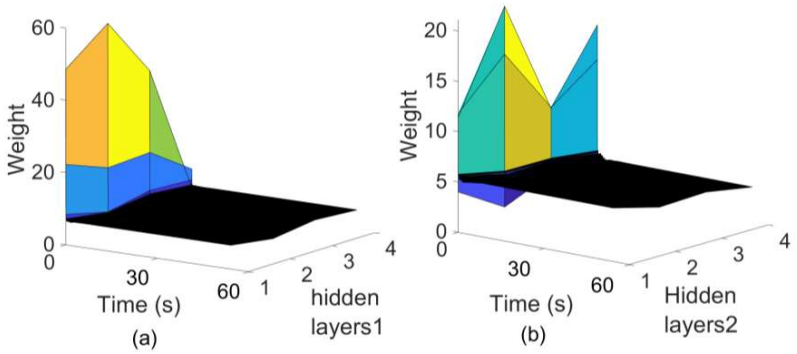

Figure 3.7. Hidden Layer response for function (a) $b_1(\mathcal{Z}_1)$ (b) $b_2(\mathcal{Z}_2)$.

The stabilized IEEE 39 bus system model is simulated using ECRNN which is applied at generator $G8$. In the ECRNN configuration all corresponding weights are updated online to estimate the power system dynamic nonlinearity as per their adaptive law (*3.39*)-(*3.42*) and (*3.54*)-(*3.57*). All diagonal matrices G_ω are updated as per (*3.10*)-(*3.13*). Corresponding state errors of generator $G8$ are shown in Figure *3.6*. For estimation of function $b_1(\mathcal{Z}_1)$ and $b_2(\mathcal{Z}_2)$ in the proposed ECRNN scheme, variation in the hidden layer is observed and depicted in Figure *3.7*. In the simulation of fault cases, three-phase short circuit faults are applied, initiated at $t = 30\ sec$ and cleared at $t = 30.2\ sec$.

Case 1: In this case, a three-phase short-circuit fault at the terminal of generator $G8$ is applied from $t = 30\ sec$ to $t = 30.2\ sec$. Under this severe fault, the response of generator $G8$ states are observed and depicted in Figure *3.8*. The proposed scheme is compared with the adaptive backstepping control (ABC) scheme and a finite time fractional-order sliding mode control (FTFOSMC) as provided in [42] and [43], respectively. In the machine state response, it is observed that the proposed scheme has reduced oscillations and fast convergence compared to the schemes [42] and [43].

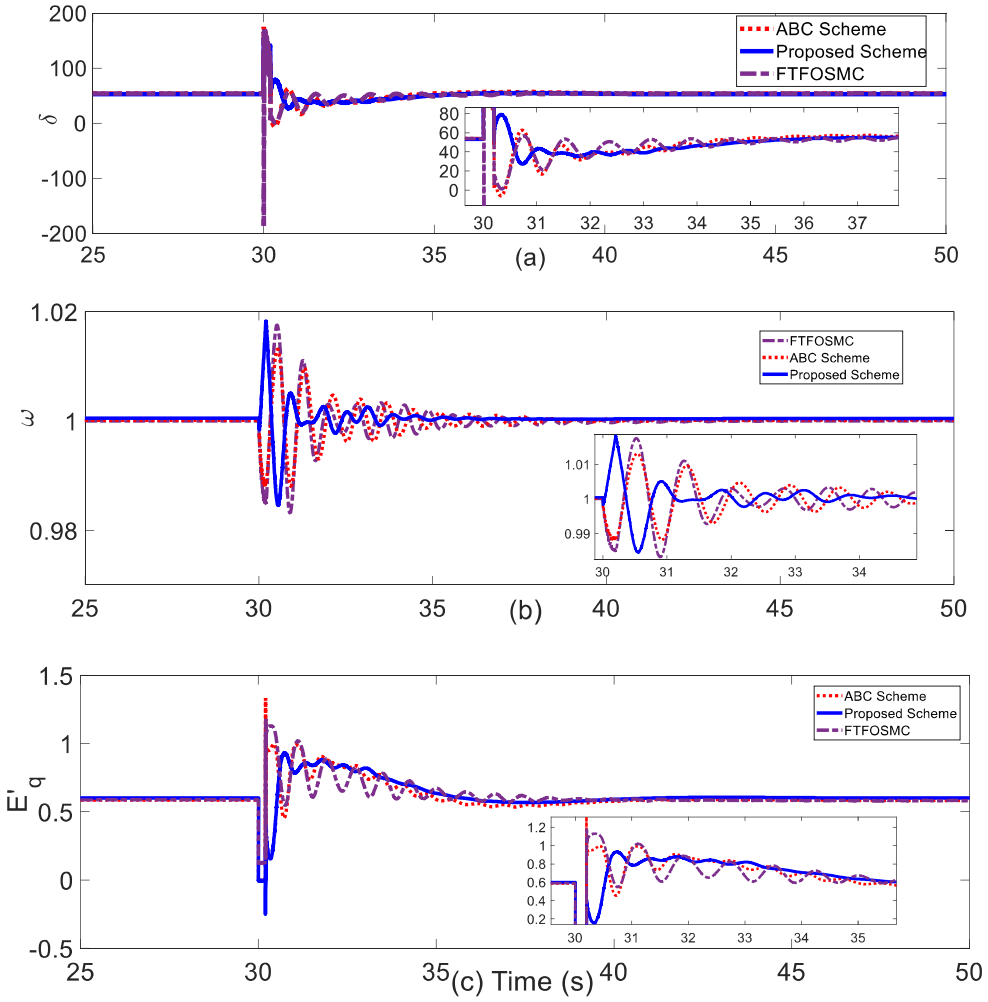

Figure 3.8. Generator G_8 state response under case-1 (a) δ (b) ω (c) E'_q.

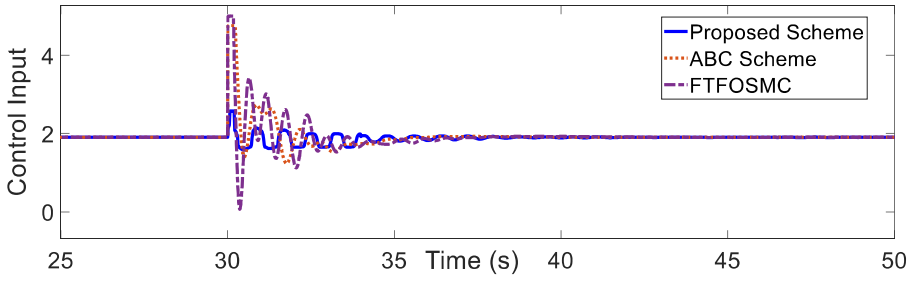

Figure 3.9. Control input response under case 1.

The rotor angle and speed response, respectively, shown in Figure *3.8* (a) and (b), oscillate during a fault and gradually decay to settle at the pre-fault position after clearance of fault. Due to the proposed ECRNN-based backstepping control performance, the multimachine state deviation is suppressed and settled to its pre-fault values more quickly

than in the schemes [42] and [43]. A similar response of machine state quadrature voltage E'_q is observed and shown in Figure 3.8(c). As in [43], the heuristic tuning of α and β parameters affect the controller performance in terms of achieving accurate control gain, although the chattering in the SMC law is significantly reduced. Also, designing an exact sliding surface from the error states for an interconnected power system network is challenging. Therefore, the control expression in [43] is complex and involves many machine signals.

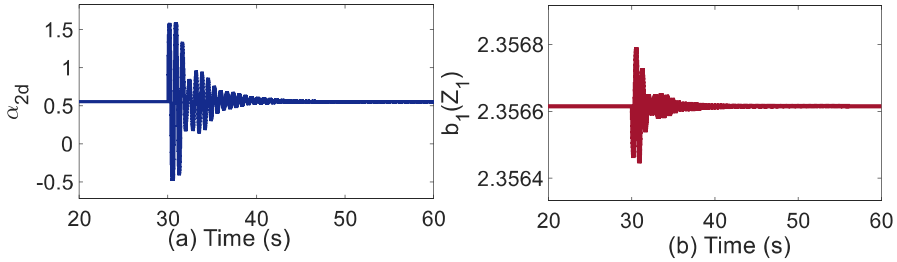

Figure 3.10. Response under case 1 (a) α_{2d} (b) $b_1(\mathcal{Z}_1)$.

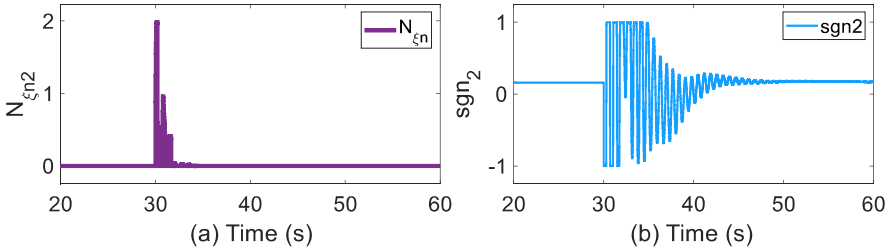

Figure 3.11. Fault case 1 (a) $\mathcal{N}_{\epsilon,n}(z)$ (b) $sgn_{\epsilon,n}(z)$.

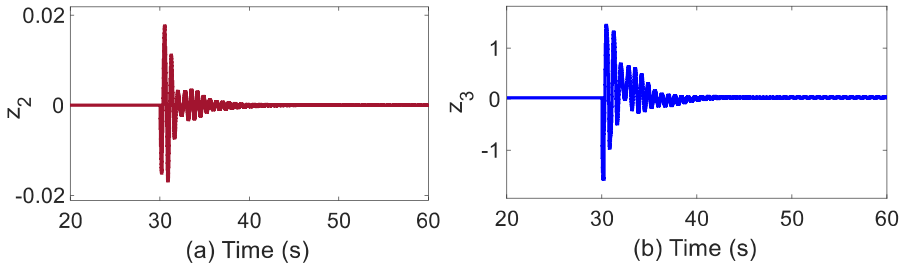

Figure 3.12. Generator G_8 state errors response under case 1 (a) z_2 (b) z_3.

The impact of the estimation of power system nonlinearity through the ECRNN is reflected in the control signal shown in Figure 3.9, as the proposed scheme requires the least control effort due to simplification in the control expression. Control expression of the proposed method involves minimum machine parameters compared to the schemes

[42] and [43], which reduces the additional signal-sensitive magnitude of these parameters. Virtual control input α_{2d} as per eqn. (2.36) is obtained and shown in Figure *3.10* (a), whereas the power system nonlinear function $b_1(\mathcal{Z}_1)$ is estimated through the proposed ECRNN scheme as illustrated in Figure *3.10* (b). The corresponding response of $\mathcal{C}^n$-Class function $\mathcal{N}_{\mathfrak{c},n}(\mathfrak{z})$ and $sgn_{\mathfrak{c},n}(\mathfrak{z})$ is shown in Figure *3.11*(a) and (b), respectively. Machine state error response for the terminal fault at generator $G8$ is shown in Figure *3.12*.

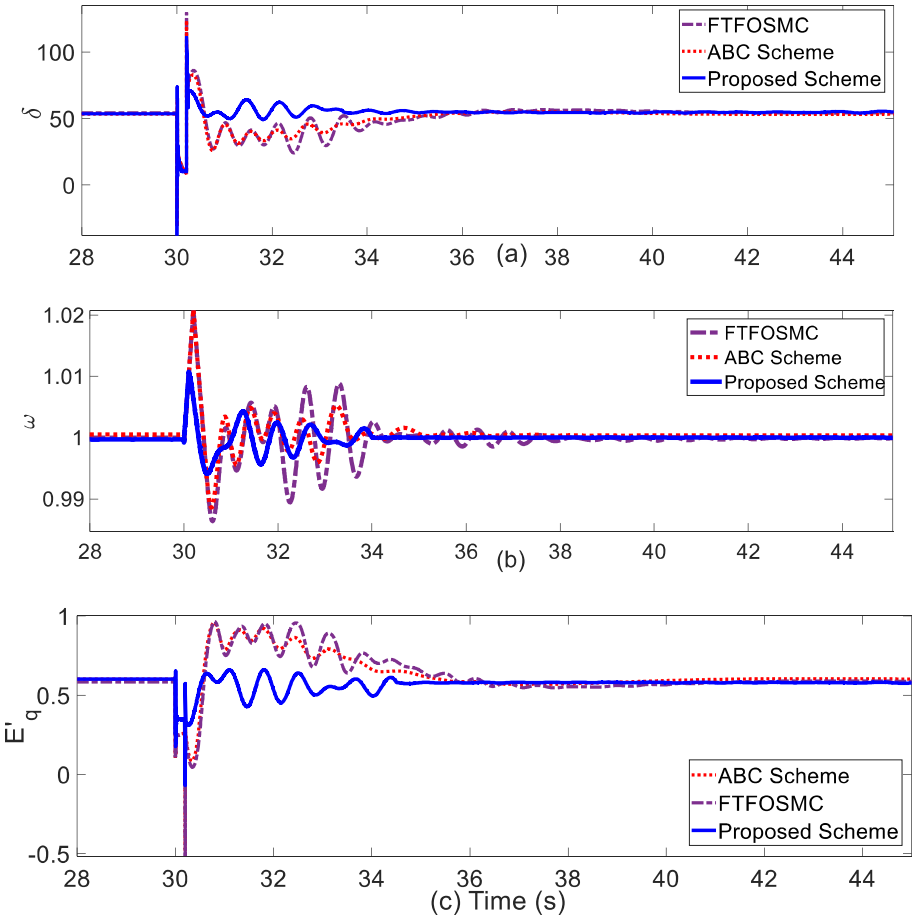

Figure 3.13. Generator G_8 state response under case-2 (a) δ (b) ω (c) E'_q.

Case 2: A severe fault case at the transmission line connected between buses 25 and 2 is applied for $0.2\ sec$. The generator $G8$ state response of rotor angle δ, speed ω, and quadrature transient voltage E'_q are shown in Figure *3.13*. It is observed from the obtained results that under this severe fault, the proposed control scheme reflects the least deviation from the equilibrium. In contrast, control schemes [42] and [43] produce more oscillations beyond the equilibrium trajectory. The interarea oscillation in the scheme [42] and [43]

are damp out with a delay of 5 sec in comparison to the proposed scheme. The fast response of the proposed scheme is obtained due to simplification in the control input. The corresponding control signal for this case is shown in Figure *3.14*. The reduced effort is reflected in the proposed control signal response compared to schemes [42] and [43].

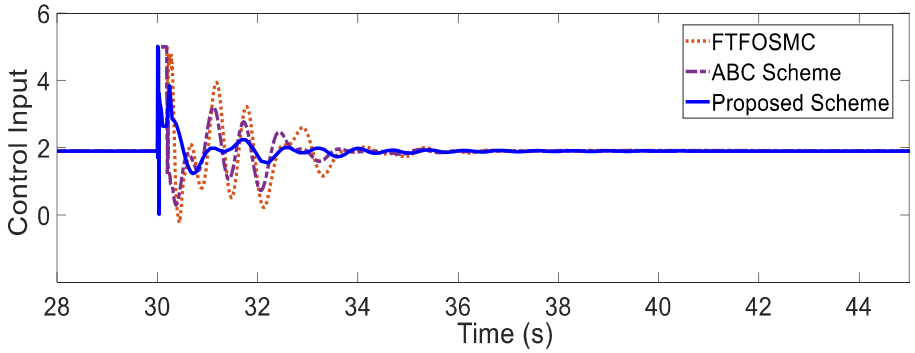

Figure 3.14. Control input response under case 2.

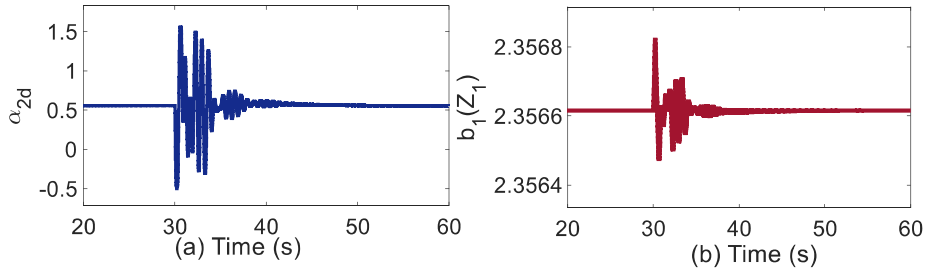

Figure 3.15. Response under case 2 (a) α_{2d} (b) $b_1(\mathcal{Z}_1)$.

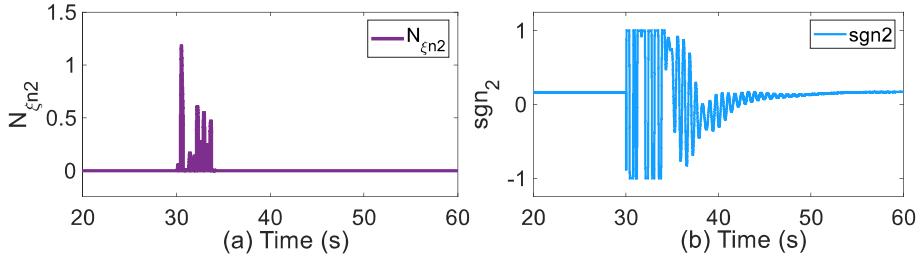

Figure 3.16. Fault case 2 (a) $\mathcal{N}_{\epsilon,n}(z)$ (b) $sgn_{\epsilon,n}(z)$.

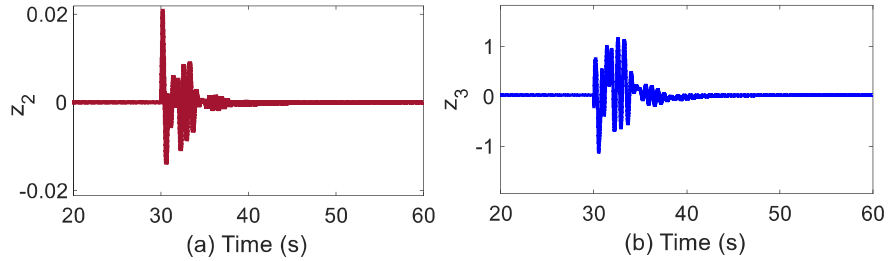

Figure 3.17. Generator G_8 state errors response under case 2 (a) z_2 (b) z_3.

The impact of ECRNN algorithm to estimate nonlinear power system terms is reflected in the obtained state responses of the generator in the form of least overshoot and fast convergence. ECRNN scheme compensates for large fluctuations through the adaptive weight update law provided by the eqns. (*3.39*)-(*3.42*) and (*3.54*)-(*3.57*). Virtual control response α_{2d} which mimics the quadrature transient voltage E'_q is depicted in Figure *3.15* (a), whereas the power system nonlinear function $b_1(\mathcal{Z}_1)$ as per the ECRNN estimation law (*3.31*) is shown in Figure *3.15* (b). The response of $\mathcal{C}^n$-Class function $\mathcal{N}_{\mathfrak{c},n}(\mathfrak{z})$ and $sgn_{\mathfrak{c},n}(\mathfrak{z})$ under this case study is shown in Figure *3.16* (a) and (b). It is clear from the obtained results that with the reduced control effort generator's transient state response is improved. The factors affecting the fast convergence response are obtained due to the robust design of $\mathcal{C}^n$-Class continuous functions $\mathcal{N}$ and sgn as explained by eqns. (*3.14*)-(*3.15*). The corresponding variation in the generator $G8$ state errors z_2 and z_3 are shown in Figure *3.17* (a) and (b), respectively.

3.5.1. Resiliency towards external disturbance.

Case 3: In this case, the idea is to visualize the resiliency of the proposed scheme against the external disturbance that appeared in the power system network. The external disturbance in the power system can be configured as a perturbation in the mechanical power, which yields uncertainty in the generator's states. These uncertainties are modeled using step perturbation in the mechanical input power P_m. Mechanical input power is increased by 5% of the rated value for 20 sec, as depicted in Figure *3.18*. As the proposed ECRNN scheme is resilient toward the system state uncertainty, thus the proposed control design is robust against the perturbations caused by state uncertainties in the interconnected power system network.

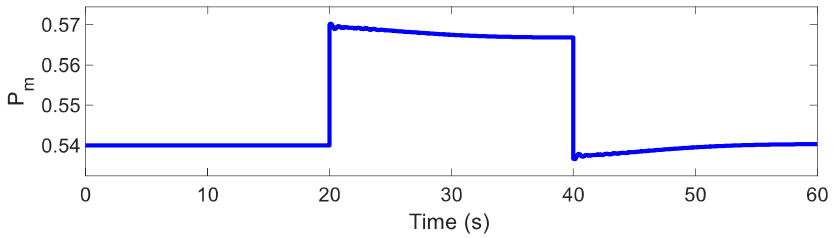

Figure 3.18. Mechanical power P_m.

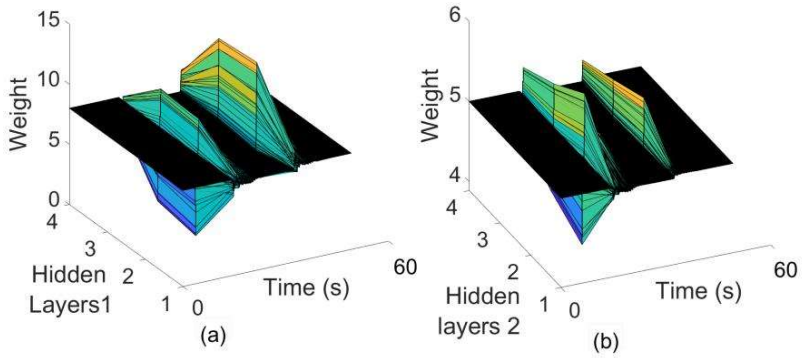

Figure 3.19. Hidden Layer response for function under case 3 (a) For the estimation of $b_1(\mathcal{Z}_1)$ (b) For the estimation of $b_2(\mathcal{Z}_2)$.

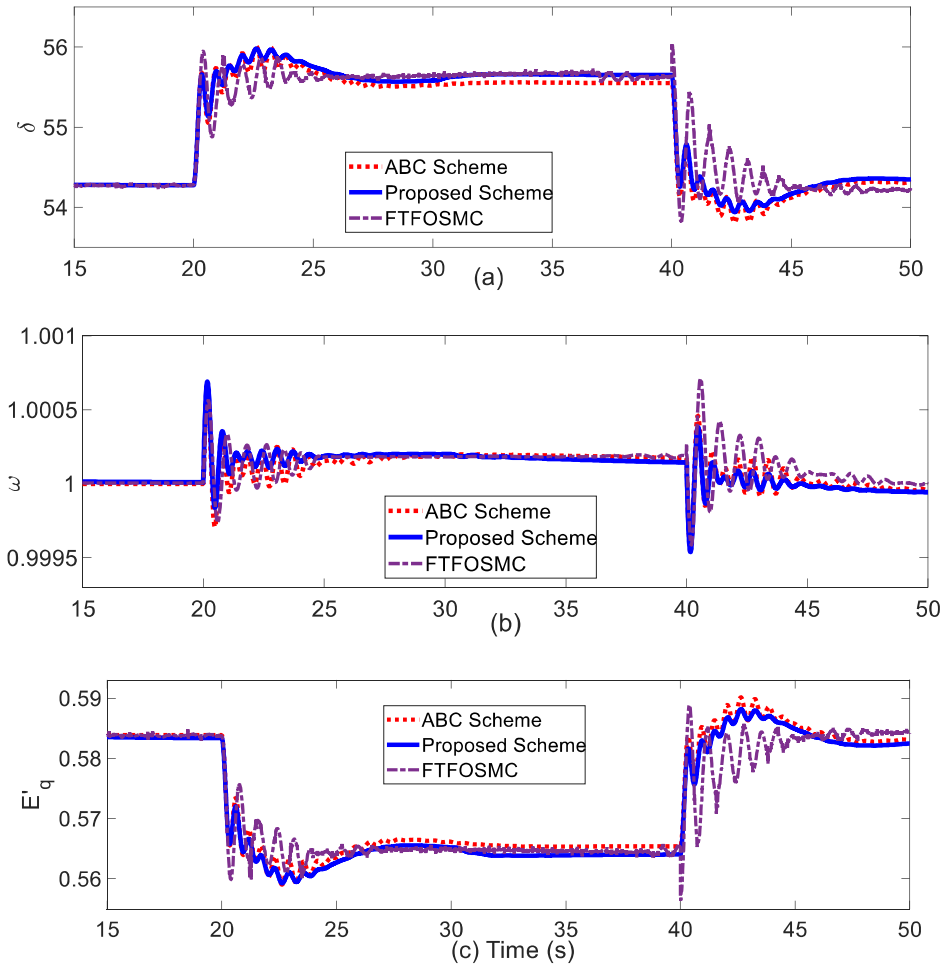

Figure 3.20. Generator G_8 state response under case-3 (a) δ (b) ω (c) E'_q.

The robustness against the state perturbation caused due to step disturbance in the mechanical input power is compensated by the adequate estimation in the variation of

unknown power system parameters and corresponding update of respective ECRNN interconnected weights. The variation of the hidden layer is observed in this case study which is illustrated in Figure *3.19*. The related compensation of uncertainty in the generator states is shown in Figure *3.20*. It is observed from the response of the generator state that the proposed scheme smoothly stabilized the state perturbation with the least fluctuation and overshoots, whereas in the methods [42] and [43], the more variation and high overshoot are obtained. The high oscillations in the scheme [43] are caused due to heuristic adjustment in the stability bound. The control input response under this case is illustrated in Figure *3.21*. The result shows the reduced transient overshoot and fast stabilization of the control signal. The enlarged view of the response of the proposed controller for this case is illustrated in Figure *3.21*. The reduced control deviation offers more stability to the generator states than the scheme presented in [42] and [43]. The corresponding variation in the virtual control input α_{2d} which mimics the quadrature transient voltage E'_q state of the generator $G8$ as per (3.36) is shown in Figure *3.22*(a). For this case study, the power system nonlinear function $b_1(\mathcal{Z}_1)$ is estimated by the ECRNN algorithm as illustrated in Figure *3.22*(b).

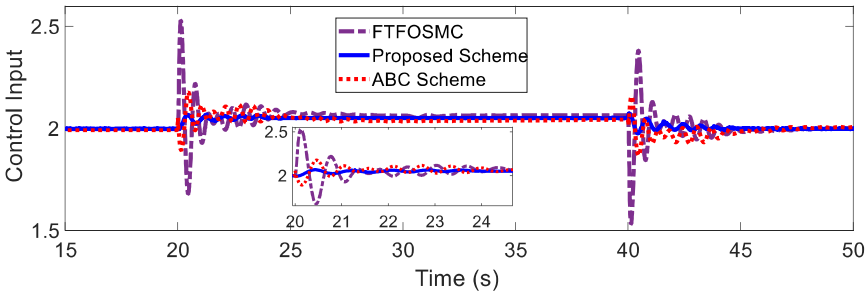

Figure 3.21. Control input response under case 3.

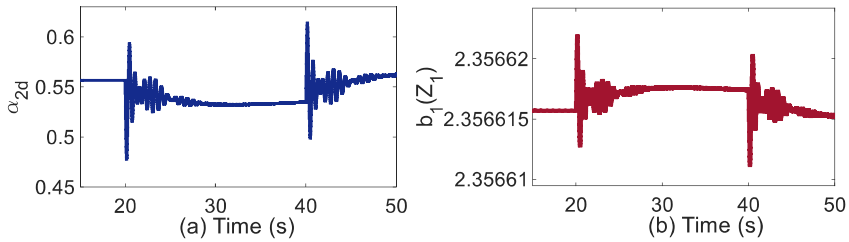

Figure 3.22. Response under case 3 (a) α_{2d} (b) $b_1(\mathcal{Z}_1)$.

3.5.2. Renewable penetration and control efficacy test.

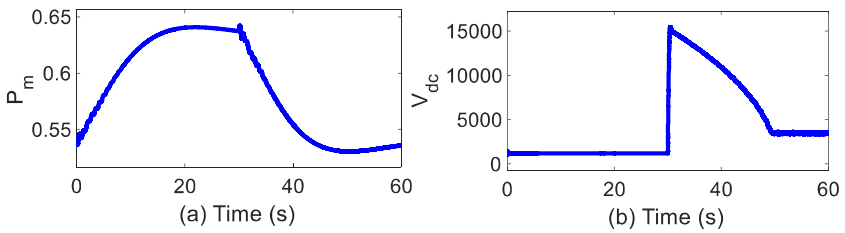

Figure 3.23. Response under case 4 (a) P_m profile (b) Interlink dc voltage V_{dc}.

Case 4: In this case, a wind turbine of a doubly-fed induction generator (WG) of 210 MW capacity is integrated with IEEE 39 bus system at bus 37, as shown in Figure *3.3*. The wind speed is taken variable from 8 to 14 m/s, pitch angle control gain is 500 with a maximum pitch angle of 45 (deg), and rate of change of pitch angle is 2 (deg/sec) is considered for the simulation. The three-phase two windings transformer and a three-phase breaker are used to integrate the WG with IEEE 39 bus system. In this case study, WG is integrated at $t = 0\ sec$, and removed at $t = 25sec$ to obtain the proposed control efficacy. Variation in the mechanical power P_m under the wind farm penetration and removal is shown in Figure *3.23*(a). The corresponding variation in the interlink dc voltage of rotor and grid side converters is depicted in Figure *3.23*(b). Both the signals P_m and V_{dc} are stabilized after the 10 se duration of the removal of the WG. Voltage and current profile at the point of common coupling (PCC) are illustrated in Figure *3.24*. The voltage profile presents the voltage drop at the removal of the wind farm because the PCC terminals are connected to the load, and the current profile attained the zero value as there is no connection with the PCC. The response of wind turbine speed is shown in Figure *3.25*, which is fluctuated at WG removal and stabilizes after 10 sec.

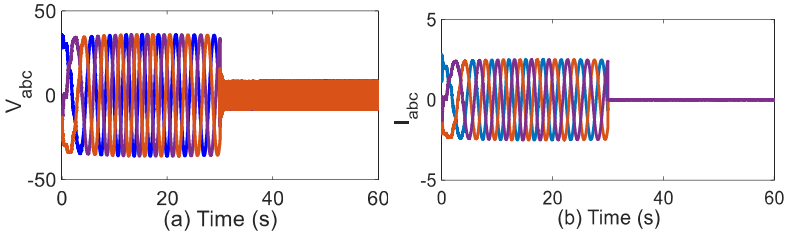

Figure 3.24. PCC terminal response (a) Voltage (kV) (b) Current (kA).

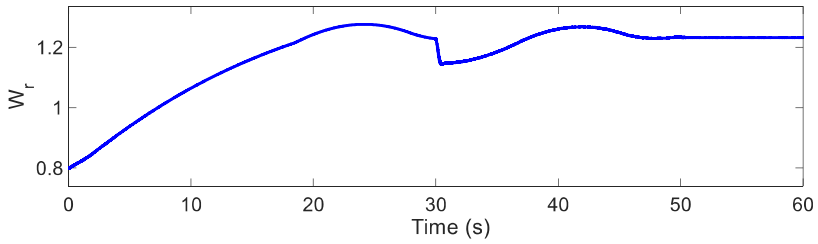

Figure 3.25. Wind turbine rotor speed.

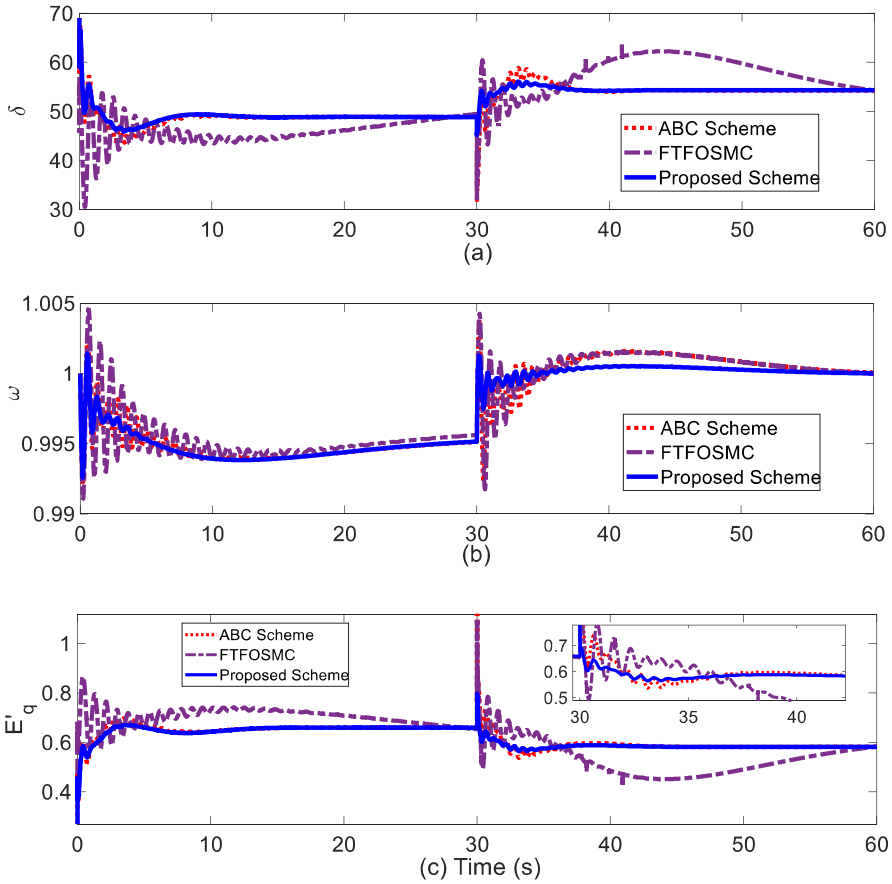

Figure 3.26. Generator G_8 state response under case-4 (a) δ (b) ω (c) E'_q.

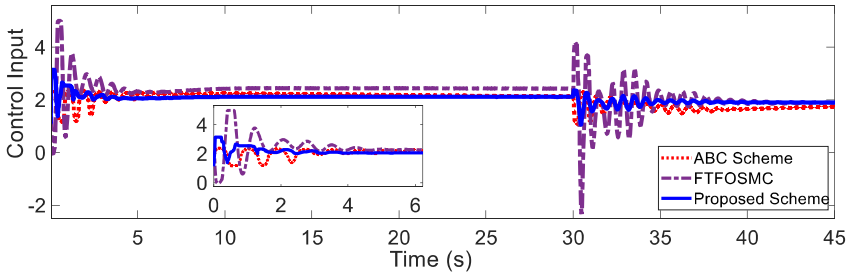

Figure 3.27. Control input response under case 4.

The corresponding variation in the generator states is illustrated in Figure *3.26*. These

results show the controller performance to achieve the global performance under the perturbations of renewable source penetration. Compared with schemes [42] and [43], the proposed control exhibits suppressed oscillations and fast convergence that stabilize the generator states with higher accuracy and smoothness. The control input response under this case is shown in Figure *3.27*. An enlarge view in Figure *3.27*shows the initial transient with better performance of the proposed scheme is compared to the schemes [42] and [43] in terms of reduced control effort. For this case study, the virtual control response α_{2d} is depicted in Figure *3.28*(a), and the power system nonlinear function $b_1(\mathcal{Z}_1)$ as per (*3.31*) is shown in Figure *3.28*(b). The response of $\mathcal{C}^n$-Class function $\mathcal{N}_{\epsilon,n}(z)$ and $sgn_{\epsilon,n}(z)$ under this case, 4 is shown in Figure *3.29*(a) and (b). These signals have represented the corresponding variations as per the fluctuations produced due to WG penetration.

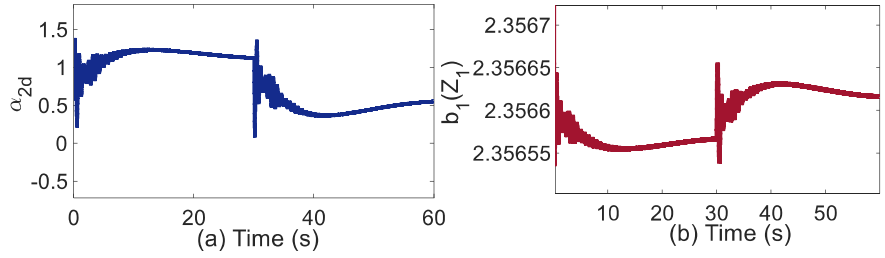

Figure 3.28. Response under case 4 (a) α_{2d} (b) $b_1(\mathcal{Z}_1)$.

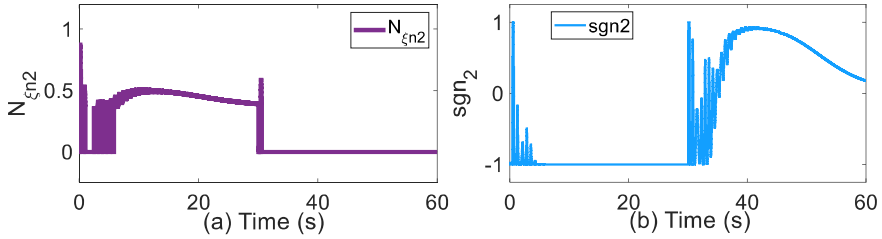

Figure 3.29. WG's integration and removal response (a) $\mathcal{N}_{\epsilon,n}(z)$ (b) $sgn_{\epsilon,n}(z)$.

3.6 Controller verification using the RTDS platform.

The validation of the proposed scheme is carried out in a real-time platform using RTDS existing in the smart grid lab at IIT BHU, Varanasi, as shown in Figure *3.31*. The NovaCor RTDS is equipped with an IBM POWER8TM processor with four cores. It can perform the software in loop (SIL) simulation with a 3.5 GHz frequency. In RTDS NovaCor chassis have PB5 type rack. Each core can simultaneously solve ninety nodes. The block diagram in Figure *3.31* explains the SIL verification process through RTDS. Simulink-

based control algorithms available in MATLAB are converted to C codes using an embedded code compiler. These C codes are dumped in the C builder tool of RTDS. The C builder creates a control block for the RTDS model. The IEEE 39 bus model available in RTDS is now used for the SIL simulation. All parameters are configured accordingly. The results are obtained in RUNTIME tool of RTDS. This way, the control scheme's real-time simulation is carried out. The following two cases are verified in real-time through RTDS.

1) A three-phase fault at $t = 2\ sec$ is applied at the terminal of generator $G8$ for $0.2\ sec$.
2) Three-phase fault between the transmission line of bus 25 and bus 37 is applied at $t = 3\ sec$ for $0.2\ sec$.

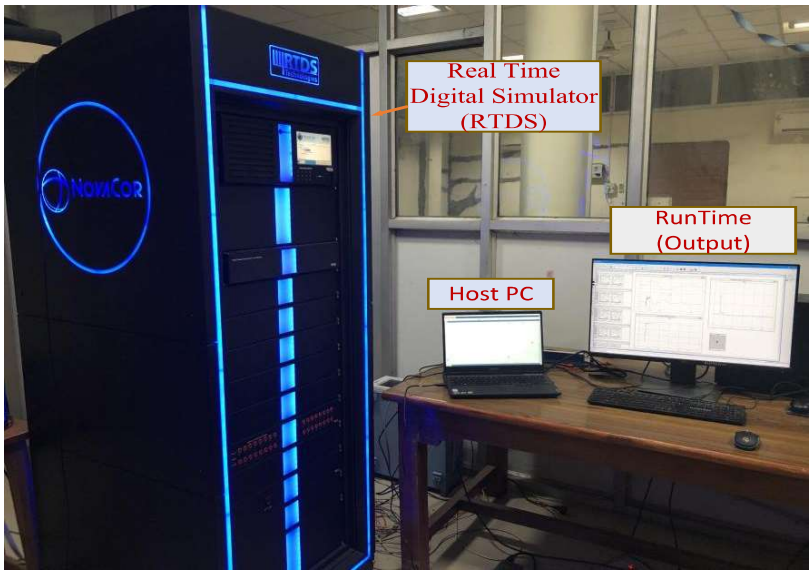

Figure 3.30. Real-time digital simulation testbed.

In the SIL verification of the proposed scheme, both faults are applied for 0.2 sec. Corresponding control signals for the three-phase short circuit faults are shown in Figure *3.32* and Figure *3.35*, respectively. The least control effort in the proposed scheme is observed due to the simplification of control expression through the ECRNN algorithm. Similarly, the proposed method shows the least overshoot and fast convergence in the state responses compared with the schemes [42] and [43], as depicted in Figure *3.33*, Figure *3.34*, and Figure *3.36*. This smooth response of states is observed due to the enhanced robustness of backstepping control and simplified adaptive tuning laws in the proposed

scheme. The results obtained in the SIL simulation verify the global performance of the proposed method.

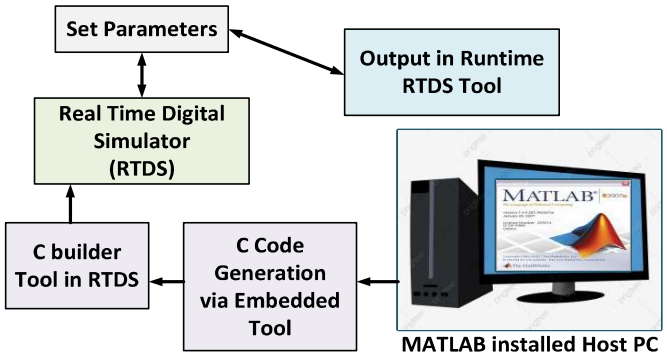

Figure 3.31. Block diagram representation of real-time test system.

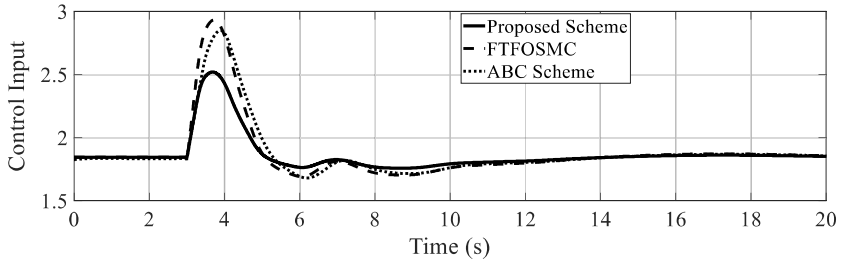

Figure 3.32. Control Input response for terminal fault at generator $G8$.

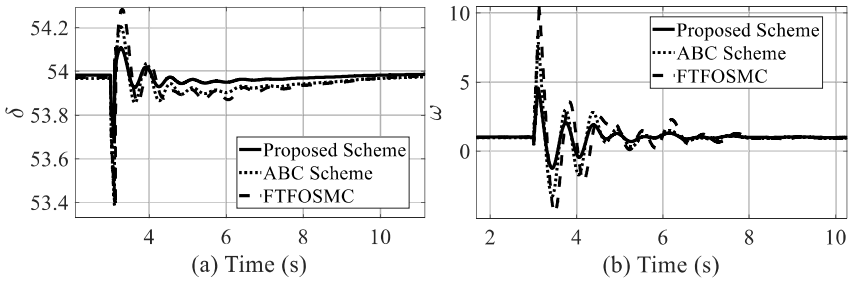

Figure 3.33. Response of generator states under terminal fault (a) δ (b) ω

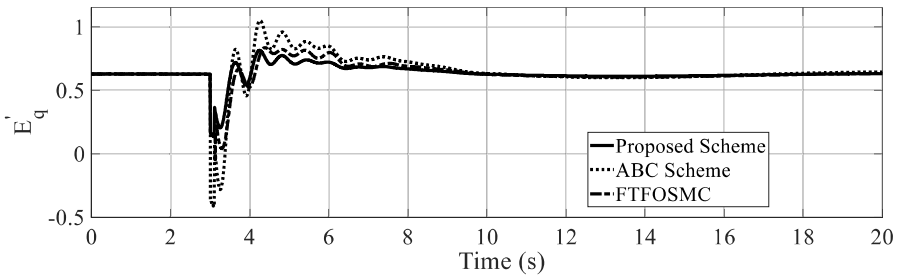

Figure 3.34. Response of generator state E'_q under terminal fault.

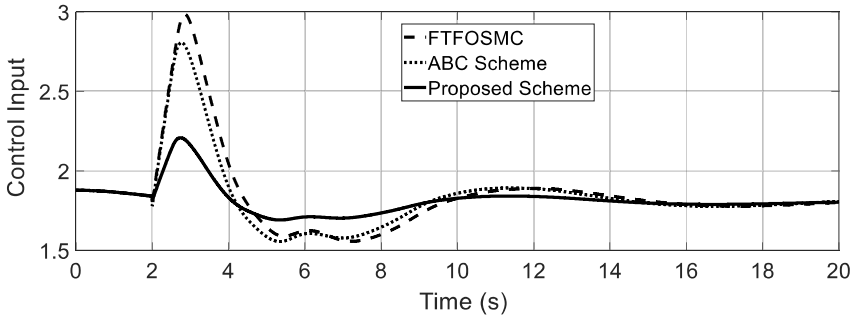

Figure 3.35. Control response for fault in between bus lines 25 and 37.

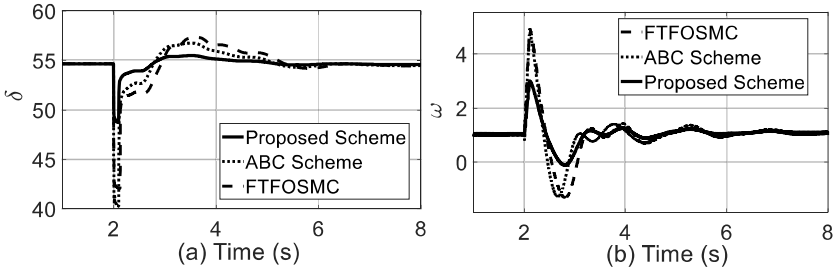

Figure 3.36. Response for fault in between bus lines 25 and 37 (a) δ (b) ω.

3.7 Summary

It was observed from the simulation study that using the proposed ECRNN-based adaptive backstepping scheme, the global stability of the generator states is achieved. The robustness against external disturbances due to the backstepping scheme was obtained during step mechanical power perturbation. An improved performance was obtained using predefined continuous differentiable functions with the precise estimation of the nonlinear control terms. The associated adaptive laws precisely updated the online weights of the ECRNN neurons under severe faults. As far as the future aspect is concerned, the proposed method can be extended to mitigate cyber issues in the power system networks. Also, a robust centralized multiagent control scheme can be designed by considering each generator as an agent.